OPTIMIZING POWER FLUID IN JET PUMP OIL WELLS

by

Kaelin Ellis

B.S. Mechanical Engineering, 2012

A Project Submitted in Partial Fulfillment of the Requirements

for the Degree of

Master of Science

in

Petroleum Engineering

University of Alaska Fairbanks

May 2025

APPROVED:

Obadare Awoleke, Committee Chair

Abhijit Dandekar, Committee Member

Ed Bueler, Committee Member

Abhijit Dandekar, Chair

Department of Petroleum Engineering

© Copyright by Kaelin Ellis
All Rights Reserved

Dedication

To Richard Cunningham (1921 - 2021)

If I have seen further, it is by standing on the shoulders of giants - Isaac Newton

Abstract

A method for optimizing power fluid to a network of jet pump wells is established. Jet pump performance is modeled by numerically solving a system of equations for specific throat and nozzle geometries. An upper boundary is established of the most efficient geometries for each well which creates a continuous function relating power fluid to oil production. Jet pump oil wells are segregated into networks which share a common power fluid surface pump. These boundaries are added together to create a non-linear objective function. To solve power fluid distribution in a network, a reduced Newton method is applied that incorporates active constraints. System constraints are that the total network power fluid is at or below surface pump capacity and that each power fluid rate is non-negative. Upon successful convergence, the power fluid estimate per well is passed to a discrete algorithm to choose between either a high or low power fluid jet pump. A computer program is developed capable of implementing the optimization method. This program is successfully tested on an eight well network, determining whether an additional well can be supported with existing equipment. The continuous optimization is fast, converging in four iterations to an answer. Any engineer can run this program, providing the benefit of a unified approach to decision making. This is a significant improvement, since no previous methods have been found in literature on how to distribute power fluid across a jet pump network.

Nomenclature

Fluid and Mechanical

$\dot{m}$	Mass Flow, lb_m/s
Ma	Mach Number
Re	Reynolds Number
$\not{V}$	Specific Volume, ft^3/lb_m
a	Speed of sound, ft/s
ρ	Density, lb_m/ft^3
A	Area, ft^2
E	Energy Density, ft^2/s^2
K	Friction Factor, unitless
P	Pressure, psia
V	Velocity, ft/s

Fluid Subscripts

di	Diffuser
ni	Nozzle Inlet
nz	Nozzle
su	Suction
te	Throat Entry
th	Throat
tm	Throat Mixture

Numerical Subscripts

i	Specific Well Reference
k	Iteration Counter
n	Total Wells in Network

Optimization

$\nabla f(q_p)$	Gradient of Obj. Function
$\nabla^2 f(q_p)$	Hessian of Obj. Function
A	Constraint Matrix
b	Constraint Vector
$f(q_p)$	Objective Function
p	Search Direction
Q_p^{pump}	Surface Pump Power Fluid
q_o	Vector of Oil Rates
q_p	Vector of Power Fluids
x	Discrete Jet Pump Selection
Z	Null Space of Constraints

Acknowledgements

No achievement in life is accomplished by one person alone; everything worth doing takes a team of support. To my partner, Alyse Loran, thank you for being my inspiration to finish my master's degree after a multi-year break. Your unwavering encouragement and belief in me kept me grounded and motivated. To my advisor, Obadare Awoleke, I am deeply grateful for your patience, candid advice, and the honest discussions we shared. I cherish all of our challenging conversations and how they helped shape my project. To my friend, Scott Pessetto, thank you for introducing me to Python, for lending an ear when I needed it, and for your constant encouragement. Your optimism was a guiding light when things were dark and progress was slow. To Ed Bueler, thank you for challenging me to see things differently. Your mastery of applied math has been a continuous source of inspiration. To my parents, Donna Valentine and William Ellis, your support has been the foundation of my success. Thank you for spending time to help me read and providing tutoring in math. I would not be where I am today without your unwavering love and guidance. To Walton Crowell, your enthusiasm for my work on jet pumps was a constant source of motivation. You made me feel that my efforts truly mattered, which fueled my drive to complete this project.

Table of Contents

List of Figures

List of Tables

Chapter 1: Introduction

Jet pumps are a very viable form of artificial lift in cold shallow reservoirs. A jet pump poses quite a few advantages over alternative methods such as gas lift or electric submersible pumps. These advantages include warming production fluid with annular heat transfer, gas handling capability, and ease of replacement. Despite these advantages, no unified method has been proposed for how to properly distribute power fluid among different wells. This becomes critical as more wells are added to existing infrastructure and the available surface pump capacity needs to be allocated.

A reliable optimization method requires an accurate system model. Despite its simple appearance, an oil well jet pump needs advanced fluid mechanics for modeling. First principle analytical models of two-phase flow in jet pumps were pioneered by Cunningham [1]. These models quantified the impact of gas handling with sonic choking at the throat entrance. Though equations derived in Cunningham's work are impeccable, assumptions used are ideal gas, incompressible and non-gas soluble liquids. These assumptions are not valid for an oil reservoir fluids mixture and more robust modeling is required.

Numerical methods are well poised to handle complex equations that cannot take advantage of simplifying assumptions. For a jet pump in an oil well, the first documented application is by Merrill, Shankar, and Chapman [2]. In this work, methods are provided for how to estimate a reservoir fluid's change in energy due to expansion and interpreting choked flow conditions. In upcoming sections, novel applications of numerical methods are introduced with multiple new algorithms. The algorithms cover topics such as calculating the minimum theoretical suction pressure of a jet pump and converging to a jet pump solution with the required inflow and outflow conditions.

The goal of power fluid optimization is to maximize total oil production from the available power fluid supply. Using standard jet pump oil well nozzle and throat combinations an upper boundary is established that relates oil production to power fluid for each well. All the boundaries together create a non-linear function with individual power fluid usage per well as the input. Upon completion, optimized power fluid rates are recommended which can be used to select specific jet pump geometries. An example concludes the paper with properly selecting power fluid rates in an eight well power fluid network.

Chapter 2: Literature Review

This literature review explores the historical evolution of jet pump modeling, particularly in the context of oil wells. This development has occurred in two distinct streams: one led by academia, which focused on accurate equations and physical modeling, and the other driven by industry engineers, who prioritized practical and timely solutions. Figure 2.1 is a timeline of the development, showing academic publications on the left and industry publications on the right. Although both academia and industry advanced jet pump technology simultaneously, there was little knowledge exchange between them. In the context of oil wells, industry models, despite their errors, were widely adopted over academic models. Only recently have the flaws in their methods been recognized and corrected.

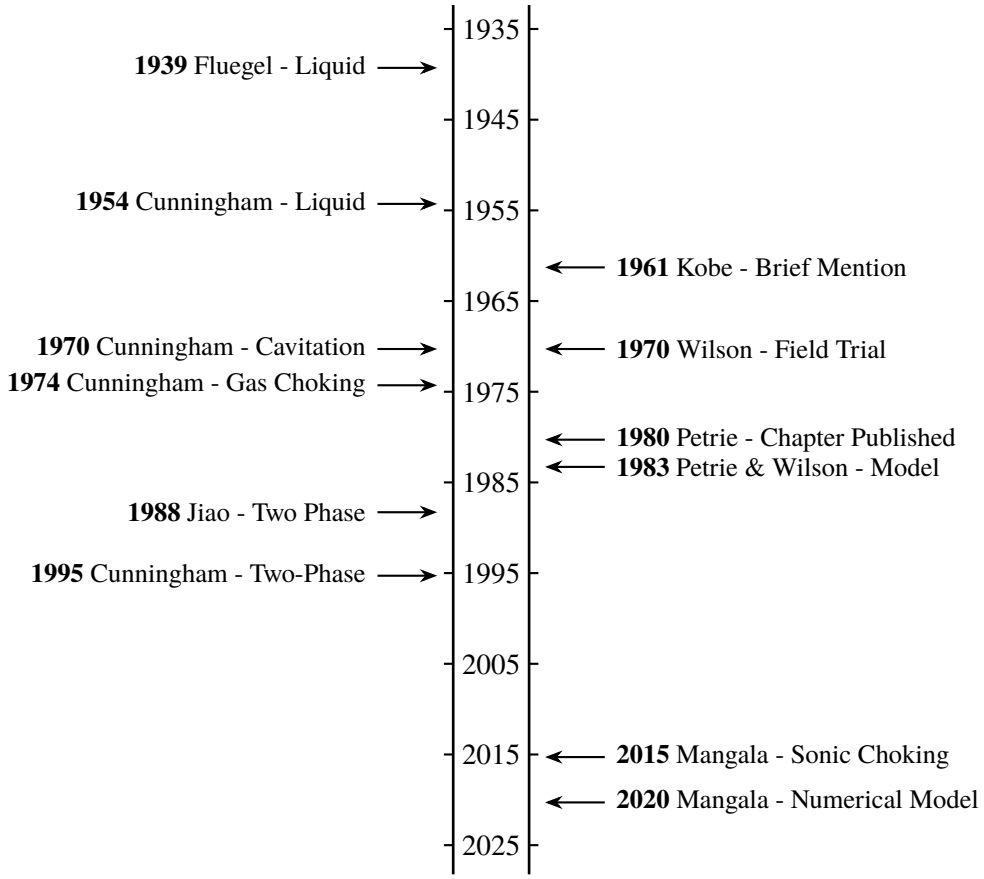

Figure 2.1: Jet Pump Research Timeline

The academic camp is represented by two notable figures: Richard Cunningham, a Professor of Mechanical Engineering at Pennsylvania State University, and Nelson Sanger, a Research Scientist

at NASA. Although they did not collaborate directly, they referenced each other's work, pushing forward the understanding of jet pump physics. On the industry side, engineers Hal Petrie, Phil Wilson, and Eddie Smart were key figures, representing the leading oilfield service companies of the time; National Production, Kobe Inc., and Guiberson. Unlike the academics, these engineers worked closely, co-authoring papers and leading projects. Petrie and Wilson, for instance, spent many years as colleagues at Kobe Inc.

The first documented reference to a jet pump from Cunningham is in a 1954 report, commissioned by the United States Air Force (USAF) [3]. Tasked with assessing the viability of jet pumps in auxiliary lube oil systems for aircraft, particularly under challenging conditions like high altitudes and viscosities, Cunningham revised existing jet pump equations. While early equations, such as those from Gustav Flugel in 1939 [4], focused on static pressure, Cunningham simplified the equations by focusing on total head pressures. His equations were widely accepted and are still in use today across various applications.

The first mention of jet pumps in oil wells appears in Kobe Oil Services Companies 1961 book, *Theory and Application of Hydraulic Oil Well Pumps* [5]. The book primarily discusses subsurface progressive cavity pumps (PCPs), but briefly acknowledges jet pumps: "The jet pump has been proposed for oil field applications and tested to a limited extent." While PCPs were effective, they struggled with high gas fractions, poor quality power fluid, and corrosive liquids, prompting Kobe Inc. to trial jet pumps in oil wells.

In 1968, Nelson Sanger at NASA conducted significant research on liquid jet pumps, publishing three reports that contributed to a deeper understanding of jet pump physics. One report provided a detailed investigation of jet pump performance under normal conditions, using 18 static pressure gauges along the pump body to develop a one-dimensional equation-based model [6]. The other two reports focused on cavitation, with Sanger proposing equations to predict the onset of this phenomenon [7]. Cunningham later built on Sanger's work, publishing a 1970 review comparing eight different cavitation models [8]. He concluded that the sigma parameter, derived by Hansen and Na, provided the best cavitation correlation. This paper is significant because it solidifies the idea that cavitation was a well understood phenomenon with wide acceptance.

In 1970, Kobe Inc. appointed Phil Wilson to lead a study on oil well jet pumps. The study involved 125 wells and focused on component reliability, efficiency, and gas handling [9]. Wilson

correctly noted that gas choked the jet pump's throat, yet he attributed performance losses to cavitation. This misunderstanding was reflected in Kobe's software, which predicted cavitation zones but failed to account for gas choking. At the time, cavitation was a primary concern in jet pump research, and no significant research had addressed jet pumps operating with both liquid and vapor phases.

In 1974, Cunningham published two key papers on liquid jets compressing gas in jet pumps. The first paper examined the throat length required for optimal mixing between liquid jets and vapor suction fluid, balancing insufficient mixing with excessive frictional losses [10]. However, the second paper was more influential, offering detailed equations for modeling two-phase jet pump behavior. Cunningham introduced the concept of sonic choking, accurately predicting performance degradation in two-phase pumps [11]. Unfortunately, despite the relevance of this research, it went largely unrecognized by oil service companies.

Hal Petrie contributed to the 1980 classic textbook *Artificial Lift Methods* [12], where he reviewed jet pump technology, but he used outdated 1934 equations by Gosline and O'Brien [13] instead of Cunningham's 1954 dynamic pressure equations. Petrie acknowledged the limitations of the cavitation model, noting that free gas contributed to choking, though the methodology he followed did not adequately address this.

In 1983, Petrie, Wilson, and Smart published a series of three articles in World Oil Magazine that became widely accepted as the definitive model for jet pumps in oil wells, despite being technically incorrect [14] [15] [16]. Their model assumed equal pressure at the suction and throat entrance of the pump, violating the first law of thermodynamics by ignoring the energy transfer required for the velocity increase through a restriction. Nevertheless, their methodology became industry standard and is still used in some modern jet pump analysis software.

The inconsistency of the Petrie, Wilson and Smart (PWS) model was discovered during the doctoral dissertation of Jiao [17] in 1988. A flow loop at the University of Tulsa was used to collect data on jet pumps with a mixture of air and water. The PWS model has a standard error of 37.2% when compared to the data, greatly over predicting the pressure differential across the jet pump. The over prediction is attributed to the PWS violating the first law of thermodynamics. Jiao publishes his own model, but relies on correlations to account for free gas instead of first principles. Despite the important information collected in his work, it is not referenced in future work by Cunningham.

Cunningham's final major contribution came in 1995, when he published a paper on liquid jets with multiphase suction (LJM) pumps [1]. Although largely theoretical, this work laid the foundation for future jet pump research in oil wells by modeling multiphase flow and highlighting the impact of sonic choking on performance. The paper's assumptions — ideal gas, incompressible liquids, and no vapor solubility — limited its applicability, but it remains a key reference for understanding multiphase jet pumps.

For two decades, industry relied on the flawed 1983 model. This changed in the early 2000s with the development of the Mangala field in Northern India, a high-porosity, high-permeability sandstone reservoir with flow assurance challenges due to wax formation. Jet pumps were used to manage the oil temperature by circulating heated power fluid. However, the software used to model jet pump performance was inaccurate. In 2015, an in-house assessment tool based on Cunningham's 1995 methodology reduced the error from 40% to under 10% [18]. Despite the significant performance improvement, the tool was developed purely in Excel and VBA which made it cumbersome to use.

In 2020, Mangala field researchers published a paper that serves as the basis for the modeling approach in this thesis [2]. They replaced Cunningham's analytical equations with numerical methods, using Python to model jet pump behavior and incorporating external vertical lift performance curves for pressure drop modeling in the tubing. This numerical approach marked a significant improvement over previous methods, but the paper lacked guidance on selecting the optimal jet pump size or optimizing power fluid.

Optimization in this study is defined as allocating a finite volume of power fluid to a jet pump oil well network. During the literature review, no papers were found that address this idea. Inspiration instead was gathered from allocating gas lift, which has been studied extensively in industry and academia.

A classical optimization method was developed for allocating gas lift by Nishikiori [19]. The method applies a quasi-Newton method for maximizing a non-linear objective function. An active set is used to handle constraints, which are incorporated into finding the search direction with a projection matrix. A gradient for each oil well on the network is calculated using finite differences. As expected with a quasi-Newton method, performance is fast. As long a reasonable starting point is provided, the method converges super-linearly. This is advantageous, as only the performance of

the oil well near assigned gas lift volumes need to be calculated, instead of performance for every possible gas lift rate.

This project takes the numerical methods from Merrill, Shankar, and Chapman [2] and optimization methods from Nishikiori [19] to develop a method for properly allocating power fluid to a network of oil wells.

Chapter 3: Jet Pump Theory

A jet pump is made up of three mechanical components which are a nozzle, throat and diffuser. Six reference locations are assigned inside the jet pump for differences in pressure and fluid properties. Reference locations are the suction (su), nozzle inlet (ni), nozzle tip (nz), throat entrance (te), throat mixture (tm) and diffuser outlet (di). Figure 3.1 provides a diagram for jet pump geometry.

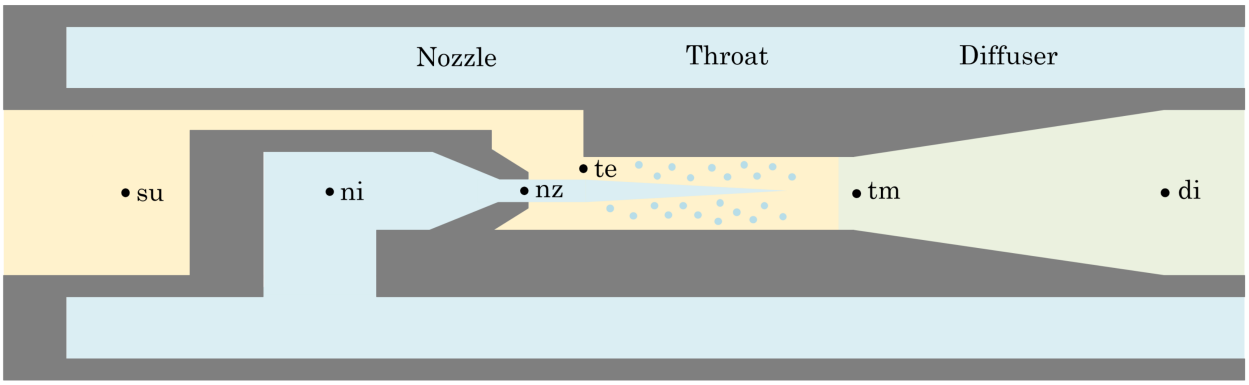

Figure 3.1: Jet Pump Overview

3.1 Fluid Energy Equation

The one dimensional fluid energy equation (3.1) provides the foundation for compressible flow in conduits [20]. The energy equation states that the differences in potential energy, pressure energy, kinetic energy, friction and work have to be equal.

$$gdz + \frac{dP}{\rho} + VdV + dF = dW \tag{3.1}$$

For a jet pump, the potential energy and work terms can be omitted. The equation simplifies to the jet pump energy equation (3.2).

$$\frac{dP}{\rho} + VdV + dF = 0 \tag{3.2}$$

Fluid flow across a jet pump nozzle tip, throat entrance and diffuser can all be modeled using variations of the jet pump energy equation. Equations associated with the different components are detailed in the next sections. Detailed derivations for these equations are provided in Appendix A,

B, C and D. Cunningham [11] also provides a useful overview of equations and their derivations for liquid jet gas pumps.

3.2 Throat Entrance

Reservoir fluids enter a jet pump by way of the throat entrance. As seen in figure 3.1 the throat entrance is constricted by the power fluid jet. An increase in velocity occurs, transforming pressure energy into kinetic energy. Reservoir fluid is a non-ideal three phase mixture with gas continually liberating from the liquid. As such, minimal assumptions can be applied to the fluid energy equation to simplify it. Only an assumption of negligible suction velocity is used. Equation (3.2), jet pump energy, is rewritten specifically for a throat entrance as equation (3.3).

$$E_{te} = \int_{su}^{te} \frac{dP}{\rho} + \frac{V_{te}^2}{2} * (1 + K_{en}) = 0 \tag{3.3}$$

$\mathrm{E_{te}}$ stands for energy of the throat entrance, calculating the difference in energy between the fluid at the suction and at the throat entrance. To have physical meaning, $\mathrm{E_{te}}$ needs to equal zero. In the application section of this paper, the integral is converted to a summation with the trapezoid rule. This allows for pressure at the throat entrance to be calculated.

3.3 Nozzle

Water is used as power fluid for flow across the jet pump nozzle. Water is incompressible and velocity at the nozzle inlet is negligible. These simplifications allow the jet pump energy equation to be analytically integrated for all the terms. Pressure at the throat entrance, $\mathrm{P_{te}}$, is equal to the pressure at the nozzle tip, $\mathrm{P_{nz}}$. These steps yield equation (3.4).

$$P_{te} = P_{ni} - \frac{\rho_{nz} V_{nz}^2}{2} * (1 + K_{nz}) \tag{3.4}$$

In practice, $\mathrm{P_{te}}$ is solved by analyzing the throat entrance. Once a numerical solution of $\mathrm{P_{te}}$ is made, the nozzle equation is used to calculate the velocity and flow rate of the power fluid.

3.4 Throat

A jet of power fluid congregates with reservoir fluids inside the throat. Momentum is transferred from power fluid into reservoir fluids, causing an increase in pressure. Mass flow, velocity and pressure at the inlet and outlet of the throat are balanced with each other. Final simplification yields equation (3.5).

$$P_{te} - P_{tm} = \frac{\rho_{tm} V_{tm}^2 K_{th}}{2} + \frac{\dot{m}_{tm} V_{tm}}{A_{th}} - \frac{\dot{m}_{nz} V_{nz}}{A_{th}} - \frac{\dot{m}_{te} V_{te}}{A_{th}} \tag{3.5}$$

Density and velocity at the throat outlet are dependent on the outlet pressure. Due to the implicit nature of the equation an iterative loop is required. The chapter on applied solutions provides detail for the secant method application to solve for $\mathrm{P_{tm}}$.

3.5 Diffuser

Kinetic energy is converted back into pressure energy at the diffuser. This results in a condition that is similar to the throat entrance. One difference though is velocity at the throat mixture is not negligible and must be included in the calculation. Solving the fluid equation for the diffuser yields equation (3.6).

$$E_{di} = \int_{tm}^{di} \frac{dP}{\rho} + \frac{V_{di}^2}{2} - \frac{V_{tm}^2}{2} * (1 + K_{di}) = 0 \tag{3.6}$$

Fluid inside the diffuser is a mixture of power and reservoir fluid, preventing analytical integration. In appendix D, the integral is converted to a summation with the trapezoid rule. This allows for pressure at the diffuser to be calculated.

Chapter 4: Oil Well Application

In the previous section equations are introduced for a liquid jet multiphase pump. Complex behavior regarding density of a reservoir fluid make an analytical solution difficult. In the following section numerical methods are introduced to provide solutions for $\mathrm{P_{te}}$, $\mathrm{P_{tm}}$ and $\mathrm{P_{di}}$. Solutions are linked backed to an oil well's inflow performance and well bore geometry to provide a solution for the entire well.

Figure 4.1 is a diagram of a jet pump inside an oil well. As shown, a jet pump has three boundary conditions to meet, which are $\mathrm{P_{su}}$, $\mathrm{P_{ni}}$ and $\mathrm{P_{di}}$. Pressure drop in the well annulus is assumed to be negligible, so nozzle inlet pressure is only dependent on the surface delivery and static pressure. Discharge pressure needs to overcome the static and frictional pressure loss in the tubing, which will be covered in a later section. Suction pressure is defined using reservoir inflow performance.

An inflow performance relationship (IPR) provides an estimate of how much fluid will be produced for a given suction pressure, also known as the wells flowing bottom hole pressure, $\mathrm{P_{wf}}$. Any method can be used to define the IPR as long as reservoir fluid flow is calculated at various bottom hole pressures. In this analysis Vogel [21] is applied for an estimate of the well's inflow performance.

4.1 Throat Entrance

Defining an initial suction pressure with an IPR provides an estimate of reservoir flow rate. For multiphase mixtures, the sonic velocity is much less than its individual components [22]. This causes jet pumps to be prone to hitting a sonic limit at the throat entrance [18]. Reservoir inflow and sonic velocity create an upper and lower boundary on the throat entry pressure. These boundaries govern the total solution for the jet pump and do not depend on any other components. The significant influence of the throat entrance make it an ideal starting point for solving the jet pump system of equations.

As previously stated, an analytical solution for the change in density of a reservoir fluid related to pressure is cumbersome. The trapezoid rule is applied to numerically find a solution of an integral [23]. In equation (4.1), trapezoid rule summation notation replaces the integral of equation (3.3).

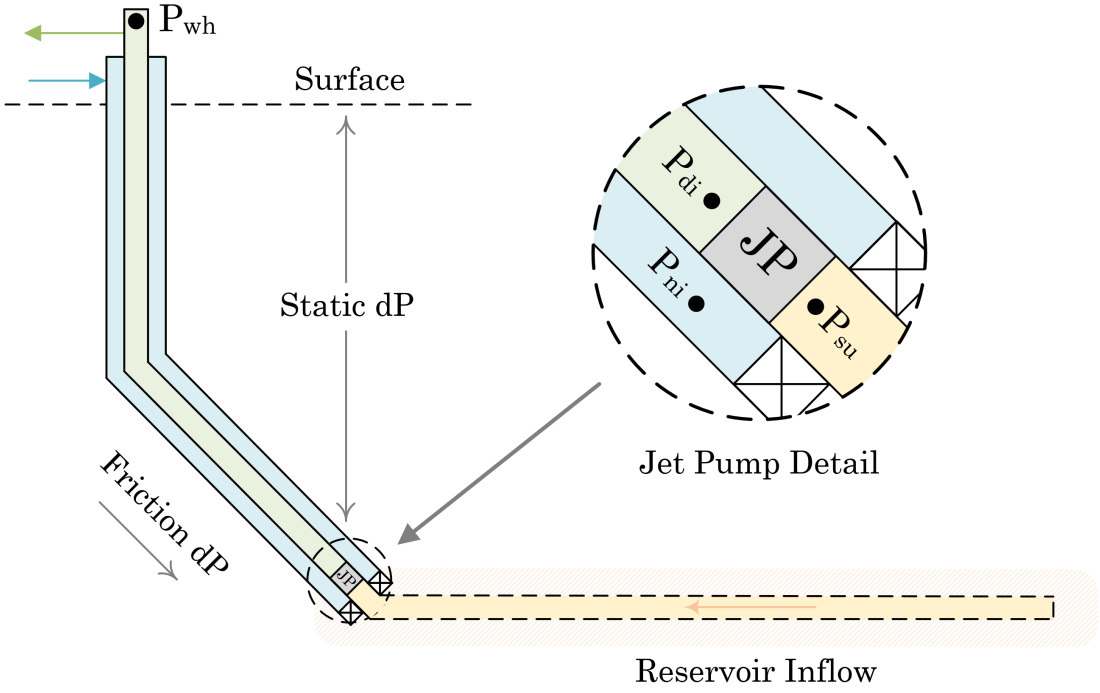

Figure 4.1: Jet Pump Well Assembly

$$E_{te} = \underbrace{\frac{\Delta P}{2}\sum_{k=su}^{te}\left(\frac{1}{\rho_k}+\frac{1}{\rho_{k+1}}\right)}_{\text{Expansion Energy}} + \underbrace{\frac{V_{te}^2}{2} * (1+K_{en})}_{\text{Kinetic Energy}} = 0 \tag{4.1}$$

Equation 4.1 is broken into two distinct portions, expansion energy and kinetic energy. Expansion describes the fluid's energy from differences in density due to pressure changes. Kinetic describes the fluid's energy from velocity and losses to friction. A solution is reached when a throat entry pressure is calculated that balances expansion energy leaving the fluid with kinetic energy entering the fluid.

Figure 4.2 is a graphical representation applying equation (4.1) to find a solution across the throat entrance. For a given well, a suction pressure is selected, which drives reservoir fluid flow rate and mixture properties. Suction pressure is viewed as the highest pressure on figure 4.2. At each iteration suction pressure is reduced by a delta pressure, ΔP, until a condition is met causing it to stop. A detailed explanation of the method and stopping conditions are shown in an algorithm below.

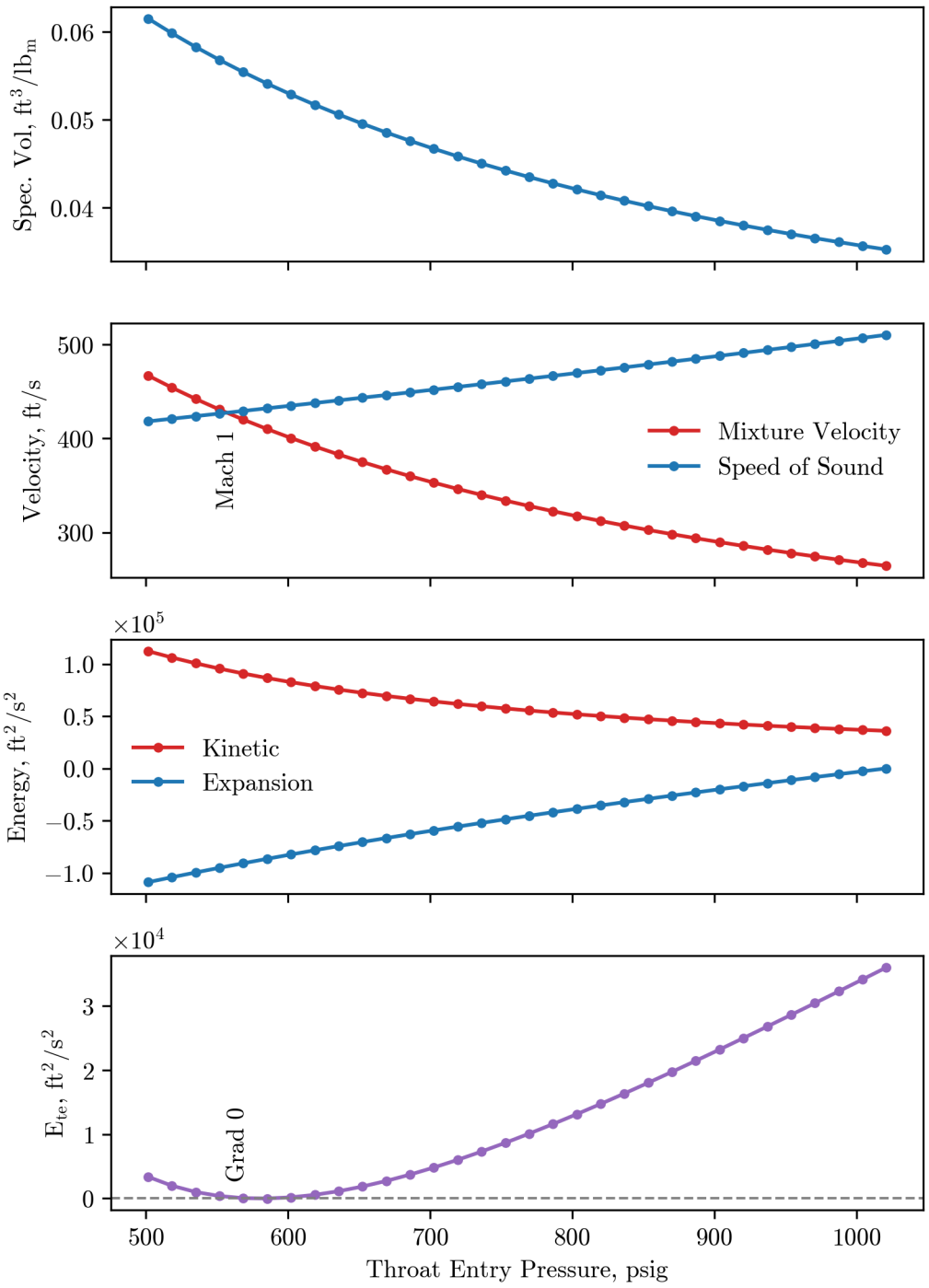

Figure 4.2: Properties for Calculating Throat Entry Pressure

Algorithm 1: Throat Entry Pressure

1. Select guess suction pressure, $\mathrm{P_{su}}$ and pressure delta, ΔP
2. $P_0 = P_{su}$
3. For $k = 0, 1, ...$
   (a) $P_{k+1} = P_k - \Delta P$
   (b) $V_{te} = V_{k+1}$
   (c) Calculate $\mathrm{E_{te}}$ and Ma
   (d) Four outcomes are possible
      i. $\mathrm{E_{te}} > 0$ and $\mathrm{Ma} < 1$. Repeat Loop, $k = k + 1$
      ii. $\mathrm{E_{te}} > 0$ and $\mathrm{Ma} \geq 1$. Stop, restart with higher suction pressure
      iii. $\mathrm{E_{te}} \leq 0$ and $\mathrm{Ma} < 1$. Stop, a non-choked solution is found. $P_{te} = P_k$
      iv. $\mathrm{E_{te}} \leq 0$ and $\mathrm{Ma} \geq 1$. Stop, a choked solution is found. $P_{te} = P_k$

In practice, pressure reductions rarely land where $\mathrm{E_{te}}$ is exactly equal to zero. Interpolation is used to calculate the pressure where $\mathrm{E_{te}}$ is zero. A smaller ΔP can be used to reduce this error but requires more computational power. In figure 4.2 a choked solution was found, where both $\mathrm{E_{te}} = 0$ and $\mathrm{Ma} = 1$. At the solution $P_{te} \approx 575$ psig. As seen in the graph of $\mathrm{E_{te}}$ at Mach one the gradient is zero. This is due to the transition from subsonic to sonic flow, represented by equation (4.2). A derivation is provided in appendix E.

$$\frac{dE_{te}}{dP} = \frac{1}{\rho}(1 - \mathrm{Ma}^2) \tag{4.2}$$

The choked solution where $\mathrm{E_{te}} = 0$ and $\mathrm{Ma} = 1$ is significant because it provides the theoretical lowest suction pressure for a given reservoir inflow and jet pump geometry. Once a jet pump is choked, no reduction in discharge pressure will result in more flow through the pump. When solving the jet pump solution, it is advantageous to start with finding the suction pressure that provides choked flow at the throat entry. The secant method is an iterative method that finds where a function is equal to zero [23]. It is well suited for finding where $\mathrm{E_{te}}$ is zero at Mach one and is shown in the algorithm below.

Algorithm 2: Lowest Theoretical Suction Pressure

1. Select two guess suction pressures P_{su}^0 and P_{su}^1.
2. Calculate E_{te}^0 at Ma= 1 and E_{te}^1 at Ma= 1.
3. For $k = 1, 2, ...$
   (a) $P_{su}^{k+1} = P_{su}^k - E_{te}^k \dfrac{P_{su}^k - P_{su}^{k-1}}{E_{te}^k - E_{te}^{k-1}}$
   (b) Calculate E_{te}^{k+1} at Ma= 1
   (c) Stop when $E_{te}^{k+1} = 0$ at Ma= 1
   (d) $k = k + 1$

Figure 4.3 is an example of $\mathrm{E_{te}}$ at five different suction pressures. The wells water cut and gas oil ratio are assumed to be constant for different suction pressures. Formation water and gas volumes are used for calculating V_{te} but are omitted in the legend to reduce clutter on the graph. Only produced oil volume at each suction pressure is displayed. Various suction pressures are equally spaced for clarity. As seen, the orange line is associated with a solution at a choked entrance, which would be found in the previously described algorithm. The green, red and purple lines cross the 0 axis prior to choking, which results in an un-choked solution. The blue line does not cross the 0 axis prior to choking, meaning the selected suction pressure was too low, resulting in too much flow.

4.2 Nozzle

A nozzle is the only jet pump component in an oil well that does not require numerical methods for its solution. A solution for $\mathrm{P_{te}}$ is obtained from the throat entrance. While a nozzle inlet pressure, $\mathrm{P_{ni}}$, is obtained using statics. With the known nozzle geometry, the required velocity and flow rate can be calculated to provide the pressure drop at $\mathrm{P_{nz}}$. This value for V_{nz} is then used in the throat solution.

4.3 Throat

The throat is inherently implicit since the properties at the outlet of the throat are dependent on $\mathrm{P_{tm}}$. The throat equation is rewritten as residual by moving parameters to the left.

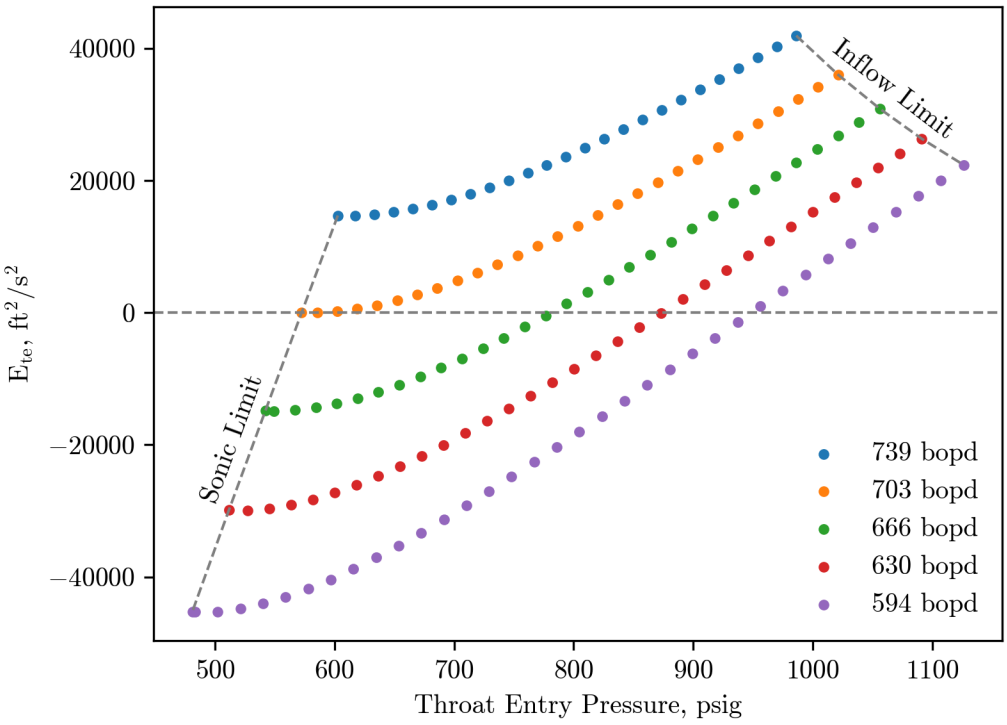

Figure 4.3: Energy of the Throat Entrance at Multiple Suction Pressures

$$R_{tm} = P_{te} - P_{tm} - \frac{\rho_{tm} V_{tm}^2 K_{th}}{2} - \frac{\dot{m}_{tm} V_{tm}}{A_{th}} + \frac{\dot{m}_{nz} V_{nz}}{A_{th}} + \frac{\dot{m}_{te} V_{te}}{A_{th}} \tag{4.3}$$

P_{tm} is iterated using the secant method until the residual is equal to zero. An algorithm demonstrating the application of the secant method for the throat is shown below.

Algorithm 3: Throat Mixture Pressure

1. $P_{tm}^0 = 1.5 * P_{te}$, calculate R_{tm}^0
2. $P_{tm}^1 = 2.0 * P_{te}$, calculate R_{tm}^1
3. For $k = 1, 2, ...$
   (a) $P_{tm}^{k+1} = P_{tm}^k - R_{tm}^k \dfrac{P_{tm}^{k-1} - P_{tm}^k}{R_{tm}^{k-1} - R_{tm}^k}$
   (b) Stop when $R_{tm}^{k+1} = 0$
   (c) $k = k + 1$

4.4 Diffuser

The diffuser is the final piece to be calculated. It is solved by approximating the integration with a summation, shown in equation (4.4). Instead of decreasing pressure until $E_{di} = 0$, pressure is increased in increments of ΔP. A diffuser also has the benefit that sonic choking is not a concern. This is due to the the large influx of water into reservoir fluid from the nozzle jet. Water drastically raises the mixture sonic velocity. A solution for diffuser pressure, $\mathrm{P_{di}}$, is obtained where $E_{di} = 0$.

$$E_{di} = \underbrace{\frac{\Delta P}{2} \sum_{k=tm}^{di} (\frac{1}{\rho_k} + \frac{1}{\rho_{k+1}})}_{\text{Expansion Energy}} + \underbrace{\frac{v_{di}^2}{2} - \frac{v_{tm}^2}{2} * (1 + K_{di})}_{\text{Kinetic Energy}} = 0 \tag{4.4}$$

Figure 4.4 is a graphical representation applying equation (4.4). The starting point of the figure is on the left at $\mathrm{P_{tm}}$, a low pressure. An algorithm below shows a method for the diffuser pressure.

Algorithm 4: Diffuser Pressure

1. Select a pressure delta, ΔP
2. $P_0 = P_{tm}$
3. For $k = 0, 1, ...$
   (a) $P_{k+1} = P_k + \Delta P$
   (b) $V_{di} = V_{k+1}$
   (c) Calculate $\mathrm{E_{di}}$
   (d) Two outcomes are possible
      i. $\mathrm{E_{di}} < 0$. Repeat Loop, $k = k + 1$
      ii. $\mathrm{E_{di}} \geq 0$. Stop, a solution is found. $P_{di} = P_k$

Like the throat entrance, the pressure iteration rarely lands where $\mathrm{E_{di}}$ is exactly zero. Interpolation should be used between the final two points to estimate the solution pressure of $\mathrm{P_{di}}$.

4.5 Outflow Considerations

At this point, a solution has been obtained that meets geometrical constraints of the jet pump and inflow constraints of the reservoir. Outflow conditions of the well ensure that the prescribed jet pump can lift reservoir fluids to surface. Two separate terms will be defined, the first being

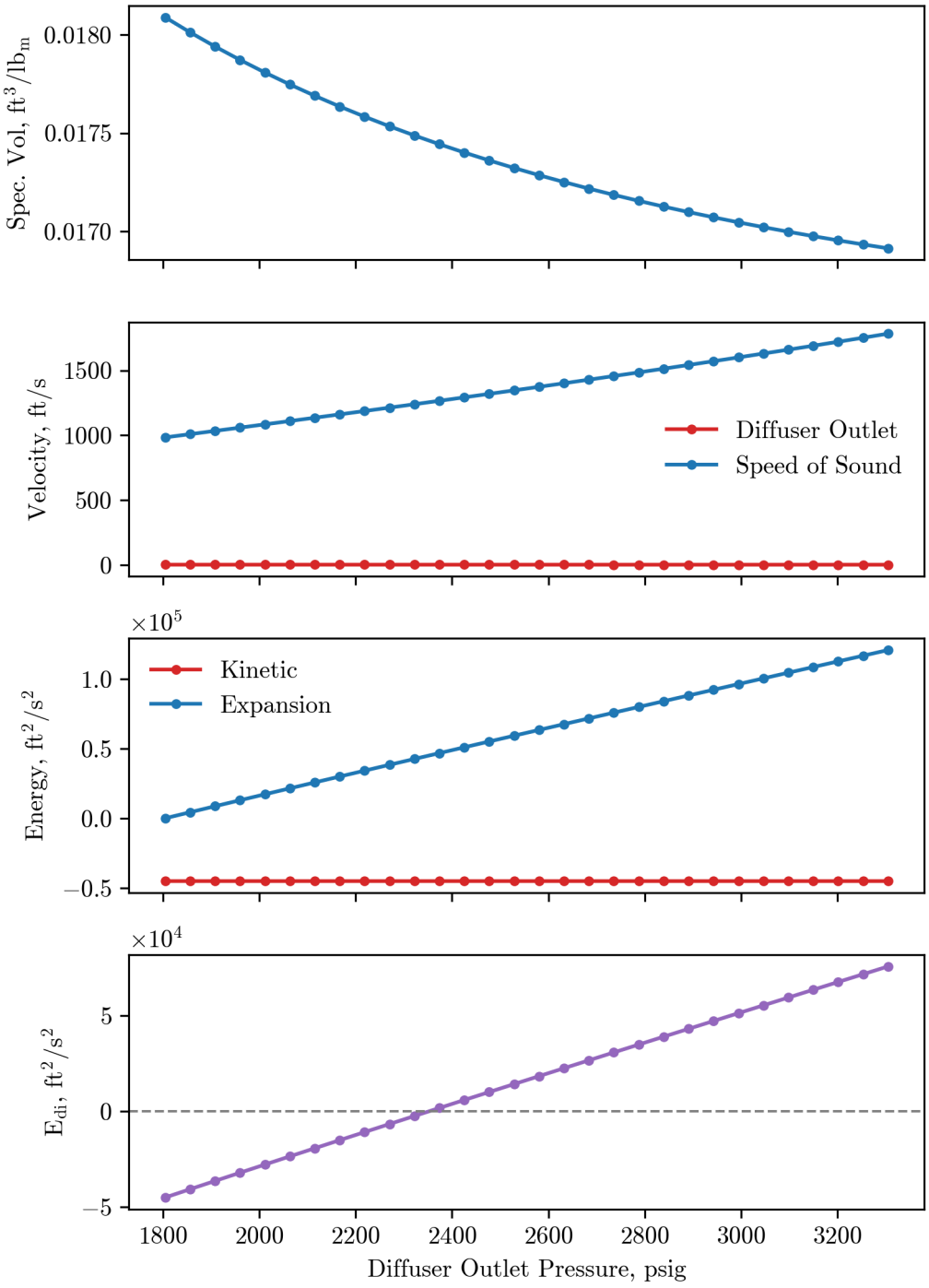

Figure 4.4: Properties for Calculating Diffuser Pressure

available discharge pressure, defined as $\mathrm{P_{di}^{A}}$. Available discharge pressure is what was calculated in the previous sections and it's how much discharge pressure can be provided for a given jet pump and inflow conditions.

The second term is required discharge pressure, defined as $\mathrm{P_{di}^{R}}$. Required discharge pressure describes pressure needed to lift the fluid from the jet pump to the well head. It includes wellhead pressure, static and frictional pressure gradient in the well. The required discharge pressure is written in equation 4.5.

$$P_{di}^{R} = P_{wh} + P_{fric} + P_{static} \tag{4.5}$$

Variables are well head pressure, frictional pressure loss in tubing and static pressure loss. Though the majority of fluid in tubing is water, free gas still exists and multiphase correlations are used. Beggs and Brill [24] is used to calculate static and frictional pressure drop. A term called discharge residual is created to compare the available and required discharge pressure.

$$R_{di} = P_{di}^{A} - P_{di}^{R} \tag{4.6}$$

For a given jet pump operating at a specific well head and power fluid pressure, discharge residual is only dependent on a pump's suction pressure. Similar to previous sections, a numerical scheme is deployed to find a suction pressure where $R_{di} = 0$. Suction pressure where $R_{di} = 0$ occurs between two extremes, the minimum and maximum. Minimum suction pressure is where the throat entrance is operating in choked flow. Maximum suction pressure uses a ten psi draw down across the reservoir. An algorithm for finding where the residual is zero is detailed below.

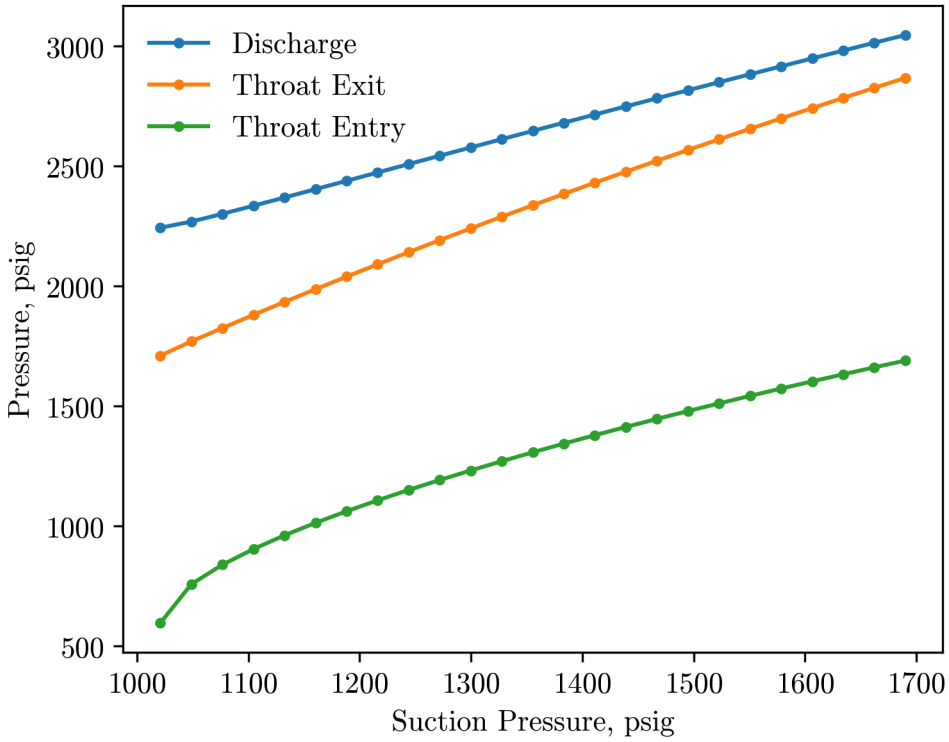

Figure 4.5: Pressure Relation from Varying Suction Pressure

Algorithm 5: Solution for Jet Pump Oil Well Assembly

1. Calculate P_{su}^0, Suction pressure of a choked jet pump
2. Calculate R_{di}^0
   (a) If $R_{di}^0 \geq 0$, Stop, a choked solution is found.
3. Calculate $P_{su}^1 = P_{re} - 10$, Reservoir pressure with 10 psig of drawdown.
4. Calculate R_{di}^1
   (a) If $R_{di}^1 < 0$, Stop, well cannot flow to surface.
5. For $k = 1, 2, ...$
   (a) $P_{su}^{k+1} = P_{su}^k - R_{di}^k \dfrac{P_{su}^k - P_{su}^{k-1}}{R_{di}^k - R_{di}^{k-1}}$
   (b) Stop when $R_{di}^{k+1} = 0$
   (c) $k = k + 1$

Figure 4.5 shows the relationship between suction pressure of the jet pump and the discharge. Despite throat entry pressure not being linear to suction, the discharge is quite linear. The secant

method takes advantage of this relationship to quickly iterate to a solution that drives discharge residual to zero. Now that a jet pump model has been completed, it can be deployed to quickly understand performance of different jet pumps in an oil well.

Chapter 5: Specific Geometry and Batch Analysis

5.1 Jet Pump Specifics

Background on jet pump nomenclature is provided to assist in continuing the discussion. Jet pumps are identified by a nozzle number and a throat ratio. In this analysis, the National standard pump geometry will be used, which are referenced in appendix H and Petrie, Wilson, and Smart [14]. Nozzle number is an integer with a value of 1 to 20, each corresponding to a specific diameter. Throat ratio is a letter of the form X, A, B, C, D or E which is throat diameter divided by nozzle diameter. An example of identification is 11X, 13C, or 9D. Table 5.1 shows numeric ratios at each letter.

Ratio	Nozzle	Throat	Area Ratio	Dia. Ratio
X	N	N - 1	2.07	1.44
A	N	N	2.63	1.62
B	N	N + 1	3.34	1.83
C	N	N + 2	4.26	2.06
D	N	N + 3	5.43	2.33
E	N	N + 4	6.90	2.63

Table 5.1: Jet Pump Throat to Nozzle Ratios

Specifying jet pumps in this manner allows quick generalities to be made about their behavior. An X pump provides the largest head, but the smallest suction flow for a given nozzle. Likewise, an E provides the smallest head, but the largest suction flow for a given nozzle. Selection of a specific nozzle number from National standard tables allows a throat to be referenced directly for a specific ratio. shown in table 5.1. For example, an 11X corresponds to an 11 nozzle with a 10 throat. A 13C would correspond to a 13 nozzle with a 15 throat.

In previous equations, frictional coefficients for jet pumps are displayed with no discussion on reasonable values. Frictional values used are based on two separate studies. First is by Sanger [6] from studying liquid jet liquid pumps. Values proposed by Sanger are in table 5.2 for the throat entrance and the nozzle. Second is by Cunningham [1] from studying liquid jet gas pumps. Values proposed by Cunningham are in table 5.2 for the throat and diffuser.

Description	Symbol	Value
Throat Entrance	K_{te}	0.03
Nozzle	K_{nz}	0.01
Throat	K_{th}	0.3
Diffuser	K_{di}	0.3

Table 5.2: Model Friction Coefficients

Live data of suction and discharge pressure gauges in a select group of wells was compared to model results using friction values in table 5.2. An adequate match was obtained comparing the model with field data to feel confident carrying the frictional values forward.

5.2 Batch Pump Runs

Assessing a single jet pump doesn't provide much context to help with optimization of the power fluid for a well. The power fluid pressure for each well can be reduced with an individual surface choke, which would reduce the power fluid rate. The problem with choking the pressure is that it wastes valuable energy required to boost the pressure up. A better approach is to replace the subsurface jet pump to meet the required operating conditions. Controlling the flow with the jet pump nozzle tip ensures that the max pressure and in turn energy, is delivered to each well.

A batch run method is used on each oil well to run an array of multiple jet pumps. If desired, every nozzle and throat combination from National jet pump standard could be ran, but this is viewed as excessive. On the North Slope of Alaska, the largest and smallest jet pump sizes are 14C and 8B respectively. For the batch run the nozzle sizes are seven to sixteen and the throat ratios are X, A, B, C, D and E. This ensures all potential combinations are covered and provides edge cases.

Result of a batch run for a well on the North Slope is shown in figure 5.1. Jet pumps are segregated into semi-finalist, red dots, and eliminated, blue dots. Jet pumps are deemed a semi-finalist if no other jet pump can make more oil for less water produced. This ensures any additional power fluid, also known as lift water, will yield more oil for a given jet pump. A curve is fitted along semi-finalists which provides an analytical equation to describe the increase in oil rate for a given power fluid volume. The curve fit is shown as equation (5.1).

$$q_{oi} = c_{1i} - c_{2i} \exp\left(-q_{pi} c_{3i}\right) \tag{5.1}$$

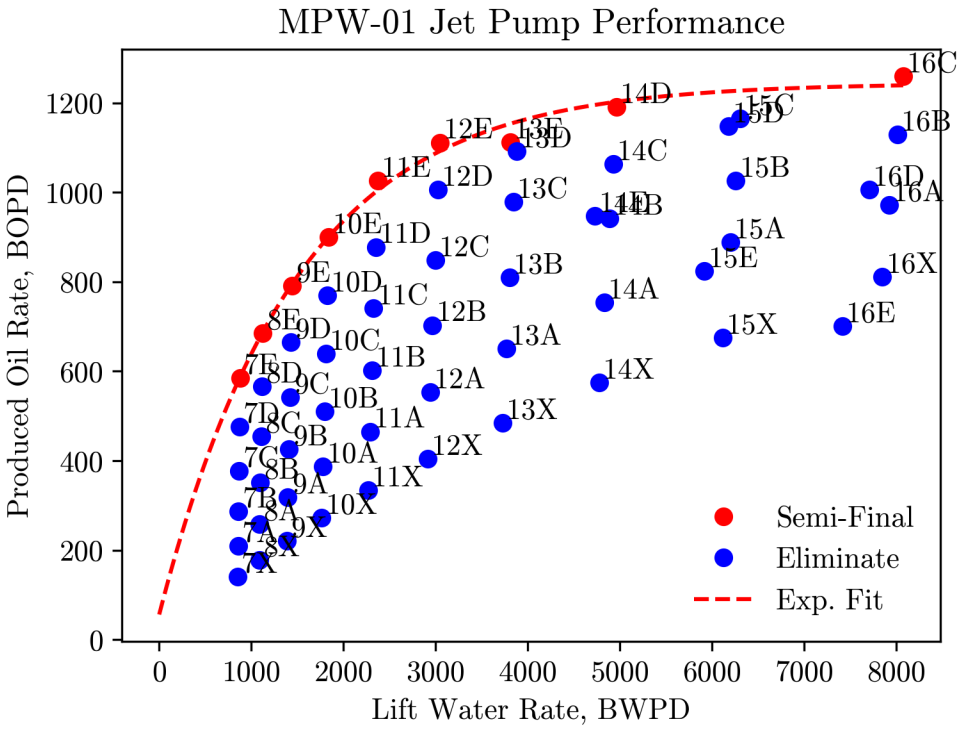

Figure 5.1: Batch Run Results

Coefficients c_1, c_2 and c_3 are found with a non-linear curve fit. The benefit of the curve fit is that a derivative can easily be taken, equation (5.2), to describe marginal increase in oil rate for a marginal increase in power fluid.

$$\frac{dq_{oi}}{dq_{pi}} = c_{2i}c_{3i}\exp\left(-q_{pi}c_{3i}\right) \tag{5.2}$$

Figure 5.2 is visual representation of the derivative of the curve fit. Above a certain jet pump size for an oil well, not much additional oil is produced for additional water spent. The dots represent the numerical derivatives at each point, which is the finite difference between the previous discrete jet pump and its self. The dashed line represents the derivative of applying an analytical description of the oil produced for water rate. The analytical curve fit provides a decent approximation of the numerical fit.

How to analytically represent each oil well has been described. A network is described which represents a series of jet pump oil wells. Optimization is applied to this network to allocate power fluid to each well.

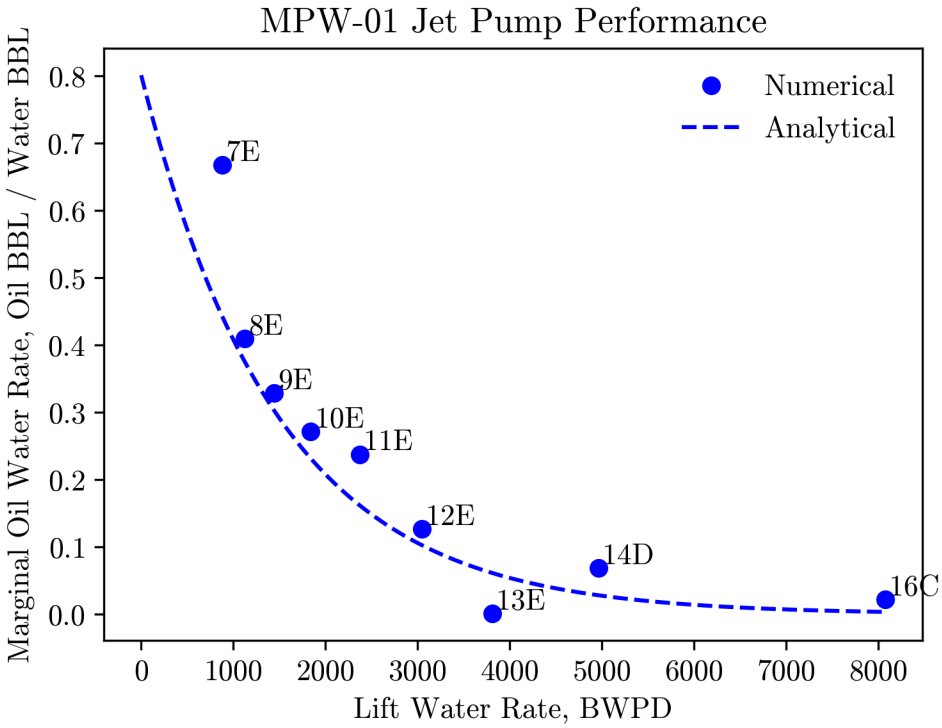

Figure 5.2: Batch Derivative Results

Chapter 6: Network Optimization

A jet pump network is defined as a collection of oil wells that share a surface power fluid pump. The power fluid pump is responsible for taking spent power fluid from a well and increasing pressure to be reused. Depending on the installation, these pumps normally operate at max capacity. Figure 6.1 shows a network of four jet pump wells that are reliant on the same surface pump. The optimization objective function and constraints take the form:

$$\text{maximize } f(q_p) = \sum_{i=1}^{n} q_{o\,i}$$

$$\text{subject to } \sum_{i=1}^{n} q_{p\,i} \leq Q_{\text{p}}^{\text{pump}}$$

$$q_{p\,i} \geq 0$$

Index i represents a specific unique oil well that is on the network, with n being the total number of wells. Vector q_p represents the individual power fluid to each well $q_p = (q_{p\,1}, q_{p\,2}, ..., q_{p\,n})^T$. Power fluid supplied to each well must sum up to less than or equal the surface pump capacity and each power fluid must be non-negative.

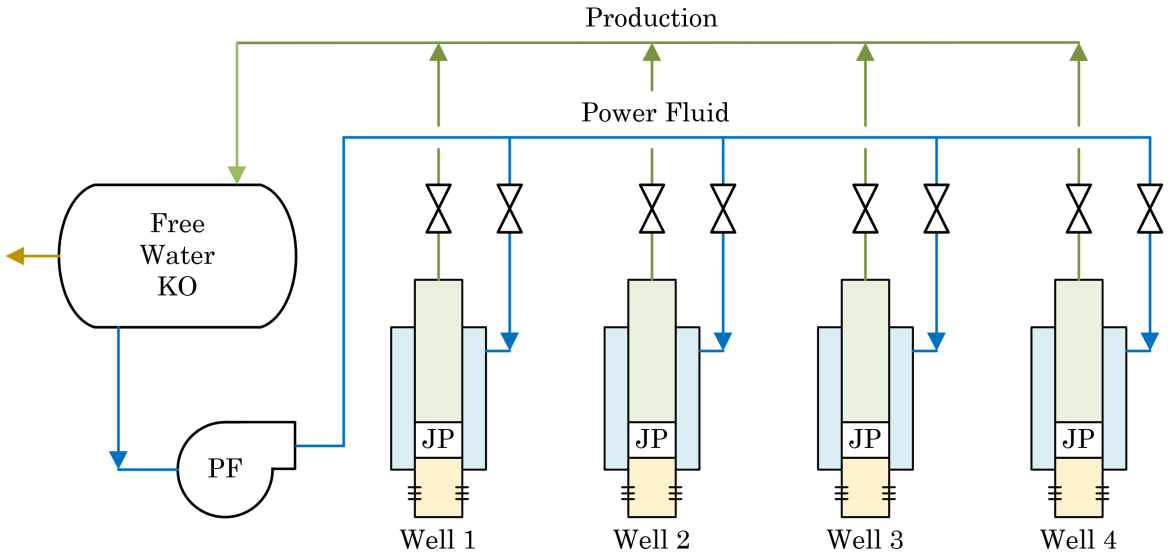

Figure 6.1: Network Diagram of Four Wells

6.1 Reduced Newton's Method with Active Set Constraints

A reduced Newton method is used for finding direction, while an active set is used to handle constraints. The active set method is solving a problem of the form:

$$\text{minimize } f(x)$$
$$\text{subject to } \hat{A}x = \hat{b}$$

The function $f(x)$ is any non-linear function while $\hat{A}$ and $\hat{b}$ are the active inequality and equality constraints. The null space of $\hat{A}$ is defined as $\hat{Z}$ and is used to reduce the gradient and Hessian of the objective function. The reduction ensures travel direction, p, does not violate any currently active constraints. The reduced gradient, $\nabla\phi(v)$ and Hessian, $\nabla^2\phi(v)$ are shown using under braces. Equation (6.1) is referred to as the *reduced Newton direction*.

$$p = \hat{Z}v = -\hat{Z}(\underbrace{\hat{Z}^T\nabla^2 f(x_k)\hat{Z}}_{\nabla^2\phi(v)})^{-1}\underbrace{\hat{Z}^T\nabla f(x_k)}_{\nabla\phi(v)} \tag{6.1}$$

A backtracking line search from Armijo [25] is used to estimate a step size that guarantees descent of the objective function. The ratio test ensures that a step size does not exceed any inactive constraints. Active constraints are continually assessed with Lagrange multiples to ensure they aren't preventing further objective function minimization while remaining feasible. Using results of the ratio test and Lagrange multiples, the active set $\hat{A}$, $\hat{b}$ and the null space $\hat{Z}$ are updated. The program terminates once an optimal condition is achieved, shown in equation (6.2).

$$\| \hat{Z}^T\nabla f(q_p) \| = 0 \tag{6.2}$$

Equation (6.2) shows that at the optimal condition, the vector of the objective functions gradient and the active constraints null space are orthogonal to each other. For full mathematical explanation and proofs on constrained optimization with active set, see Griva, Nash, and Sofer [26].

6.2 Jet Pump Network Application

The reduced Newton method with active constraints to a jet pump network of oil wells is now applied. Generic equations above are written specifically for a jet pump network. The objective

function is multiplied by negative one to turn it into a minimization. This allows methods from Griva, Nash, and Sofer [26] to be applied since all problems in the text are minimized.

$$\begin{aligned} \text{minimize } f(q_p) &= \sum_{i=1}^{n} -c_{1i} + c_{2i} \exp\left(-q_{pi} c_{3i}\right) \\ \text{subject to } & \sum_{i=1}^{n} q_{p\,i} \leq Q_{\text{p}}^{\text{pump}} \\ & q_{p\,i} \geq 0 \end{aligned}$$

Gradient of the objective function is a first derivative of each well with respect to its own power fluid.

$$\nabla f(q_p) = \begin{pmatrix} -c_{21} c_{31} \exp\left(-q_{p1} c_{31}\right) \\ \\ ... \\ \\ -c_{2n} c_{3n} \exp\left(-q_{pn} c_{3n}\right) \end{pmatrix}$$

Hessian of the objective function is a diagonal matrix of a second derivative of each well with respect to its own power fluid.

$$\nabla^2 f(q_p) = \begin{pmatrix} c_{21} c_{31}^2 \exp\left(-q_{p1} c_{31}\right) & 0 & 0 \\ \\ 0 & ... & 0 \\ \\ 0 & 0 & c_{2n} c_{3n}^2 \exp\left(-q_{pn} c_{3n}\right) \end{pmatrix}$$

Top n rows of constraint matrix A and vector b represent individual wells. Bottom $n+1$ row represents total power fluid limitation. Bottom row is multiplied by negative one so all rows adhere to $Ax \geq b$. The letter k is an iteration counter.

$$A = \begin{pmatrix} 1 & 0 & 0 \\ \\ 0 & ... & 0 \\ \\ 0 & 0 & 1 \\ \\ -1 & -1 & -1 \end{pmatrix} \quad q_p^k = \begin{pmatrix} q_{p1} \\ \\ ... \\ \\ q_{pn} \end{pmatrix} \quad b = \begin{pmatrix} 0 \\ \\ ... \\ \\ 0 \\ \\ -Q_p^{pump} \end{pmatrix}$$

To start the optimization scheme, a feasible point must be selected. To begin, power fluid is

evenly distributed among wells following $q_{pn} = Q_p^{pump}/n$. As a result, only the bottom row is active in A and b.

$$\hat{A} = \begin{pmatrix} -1 & \dots & -1 \end{pmatrix} \quad q_p^0 = \begin{pmatrix} \frac{Q_p^{pump}}{n} \\ \dots \\ \frac{Q_p^{pump}}{n} \end{pmatrix} \quad \hat{b} = \begin{pmatrix} -Q_p^{pump} \end{pmatrix}$$

In the following application, QR factorization is used to find the null space of active constraints. Results from the QR method can also be used to find Lagrange multiples without much additional computation required. Again, Griva, Nash, and Sofer [26] should be used for details.

6.3 Pseudo Optimization Code

Pseudo code for applying the Newton method for jet pump network with active set constraints is shown below.

1. Set initial conditions:
   (a) k, iteration counter $k = 0$
   (b) q_p^0, evenly split available power fluid for each well
2. Active Constraints
   (a) Loop through each row in A and b, testing if q_p^k is active or inactive.
   (b) If active, store in matrix $\hat{A}$ and vector $\hat{b}$.
   (c) Store active constraint index in vector W.
3. Calculate first and second order conditions
   (a) $\nabla f(q_p^k)$, Gradient
   (b) $\nabla^2 f(q_p^k)$, Hessian

4. With the active constraints, calculate the following:

   (a) QR Factorization

$$\hat{A}^T = QR = (Q_1\ Q_2)\begin{pmatrix} R_1 \\ 0 \end{pmatrix}$$

   (b) Null Space

$$\hat{Z} = Q_2$$

   (c) Lagrange Multiples

$$\hat{A}_r = Q_1 R_1^{-T}$$
$$\hat{\lambda} = \hat{A}_r^T \nabla f(q_p^k)$$

5. Test for Optimality

   (a) If $\hat{Z}^T \nabla f(q_p^k) = 0$ and no constraints are active, you are optimal.

   (b) If constraints are active:

      i. If $\hat{\lambda} \geq 0$ then stop, local stationary point has been reached

      ii. If $\hat{\lambda} < 0$ drop minimum λ constraint. Update W, $\hat{A}$, $\hat{A}_r$ and $\hat{Z}$.

6. Search Direction, p using Reduced Newton Method

$$p = \hat{Z}v = -\hat{Z}(\hat{Z}^T \nabla^2 f(q_p^k)\hat{Z})^{-1}\hat{Z}^T \nabla f(q_p^k)$$

7. Step Size, α using backtracking

   The variable α is the distance to guarantee descent of the objective function.

   (a) Begin with $\alpha = 1$, check if $f(q_p^k + \alpha p) \leq f(q_p^k) + \mu\alpha p^T \nabla f(q_p^k)$

   (b) If not, reduce $\alpha = \frac{1}{2}$, check again

   (c) Continue to follow sequence: $\alpha_i = 2^{-i}$

   (d) Stop once $f(q_p^k + \alpha p) \leq f(q_p^k) + \mu\alpha p^T \nabla f(q_p^k)$

8. Step Size, τ using ratio test

   The variable τ is the distance to any inactive constraints.

$$\tau = \min \left\{ \frac{a_i^T \bar{x} - b_i}{-a_i^T p} : a_i^T p < 0, i \notin W \right\}$$

   Make note of distance to nearest inactive constraint and the associated index, i.

9. Set $\bar{\alpha}$ to the lower value of α or τ.

$$\bar{\alpha} = \min(\alpha, \tau)$$

   (a) If $\bar{\alpha} = \tau$ add constraint i. Update W, $\hat{A}$, $\hat{A}_r$ and $\hat{Z}$.

10. Update q_p^{k+1} by using $q_p^{k+1} = q_p^k + \bar{\alpha} p$.

11. Repeat step three until optimal condition found.

6.4 Example

The optimization methodology was applied at a drill site in the Milne Point field of Alaska. The location of Milne Point is shown on the map in Figure 6.2. The artificial lift method at the drill site is a mixture of electric submersible pumps and jet pumps. The drill site has its own production separator and power fluid pump which act as a jet pump network for eight wells. Several months before the analysis, a series of grass-roots production wells were drilled at the site. Based on calculations before the optimization scheme was developed, it was concluded that the network could only support eight wells on jet pump. As a result, one of the grass roots wells was completed as an electric submersible pump (esp) and the other wells as jet pumps.

During surveillance of the electric submersible pump, it was noted that its ability to draw down the well was less than it's adjacent jet pumps. The operator wanted to swap the well from electric submersible to jet pump, but did not know how other jet pump wells would be impacted. Inflow performance showed that the well could produce 1250 bopd using a jet pump. To fully understand performance, the optimization scheme was first deployed on the existing well configuration. These results are compared to adding the esp well as a jet pump.

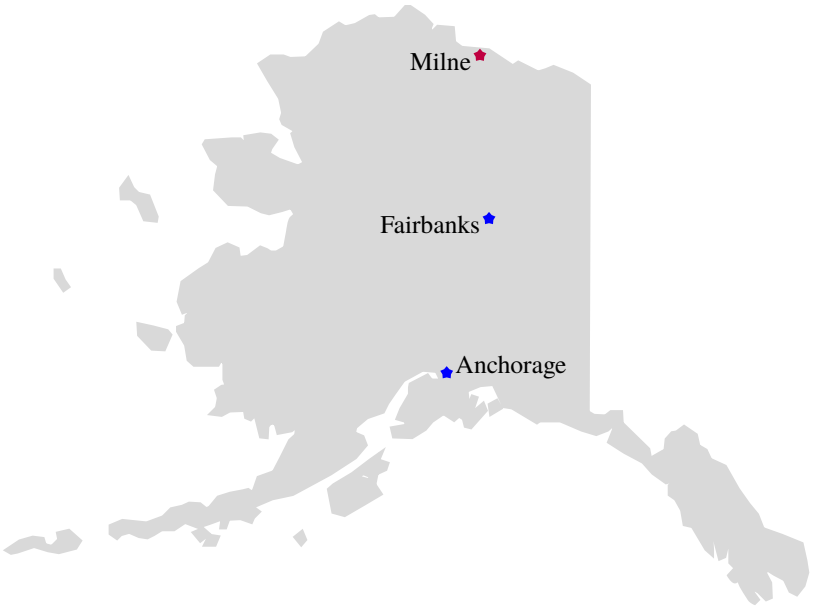

Figure 6.2: Milne Point Location

Number	Type	Size	Oil	FWC	FGOR	c1	c2	c3
15	JP	11B	274.7	49.9	1172	353.7	230.8	9.62e-4
17	JP	12B	378.3	67.6	931	578.9	430.4	5.64e-4
26	JP	13C	443.8	28.5	409	835.5	506.1	5.69e-4
27	JP	12B	734.8	18.6	341	834.5	674.0	8.63e-4
29	JP	14C	1188.4	3.5	190	1127	980.2	5.98e-4
31	JP	14C	1037.1	49.8	862	944.5	807.5	6.89e-4
33	JP	14C	1205.5	31.1	978	1237	1226	7.35e-4
36	JP	14C	1162.9	33.3	592	1262	858.6	4.63e-4
22	ESP	NA	852.2	26.2	295	NA	NA	NA

Table 6.1: Drillsite Production Wells

The surface network pump has a max capacity of 32000 bwpd with a discharge pressure of 3400 psig, which is at the max allowable operating pressure of the piping. It was decided to keep the capacity and discharge pressure of the network pump at a fixed setting in the optimization scheme to simplify the analysis. The scheme could be run at different power fluid pressures and rates, but that would complicate the problem.

6.4.1 Results

The continuous optimization scheme is first run on the base jet pump wells. Figure 6.3 shows the base jet pump wells run, where iteration 1 is starting with an even distribution of power fluid to each well. The left is the total estimated oil rate coming from the network. On the right is the optimality

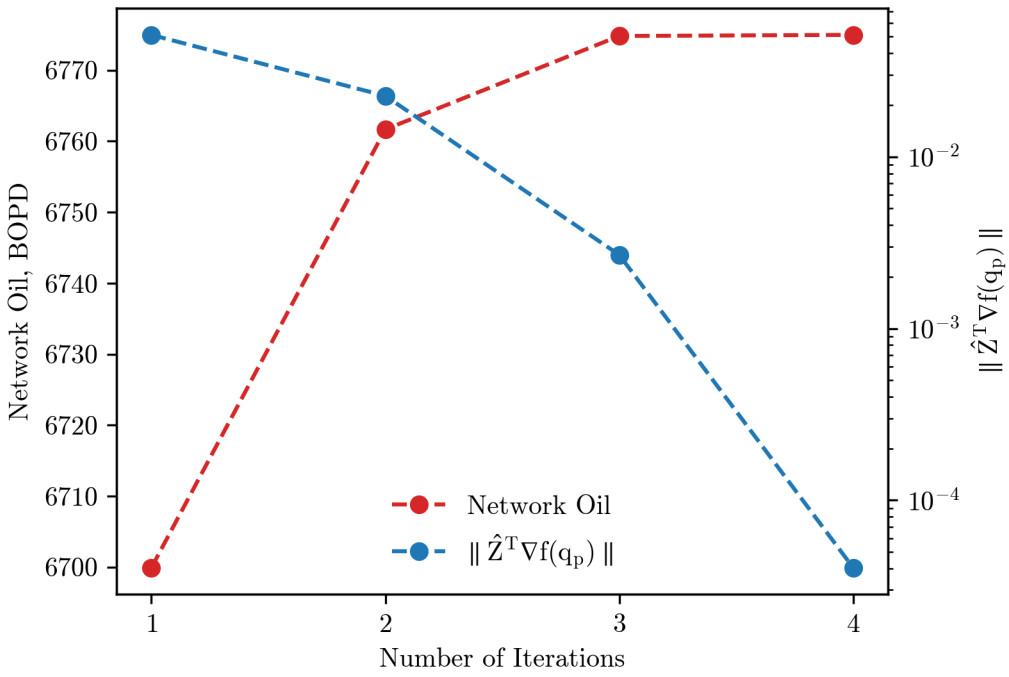

Figure 6.3: Convergence of Oil Produced and Optimality Condition

condition, shown in equation (6.2). The program terminates when the optimality condition is below a tolerance of 1E-3. The continuous optimization scheme is fast, taking advantage of the quadratic behavior of the Newton method to converge in four iterations.

The esp well is modeled as a jet pump using bottom hole gauge and well test data. Coefficients for well 22 are estimated to be c1: 1237, c2: 1226 and c3: 7.3e-4. These coefficients and modeling supported prior to ideas that the well would produce approximately 1250 bopd as an esp. The well is then added to the existing network and the continuous scheme is rerun.

Name	Eight Wells BOPD	Well 22 BOPD	Type	Total BOPD
Base Run	6774	852	ESP	7627
Conversion	6619	1176	JP	7796
Difference	-155	+324	JP	+169

Table 6.2: Network Run Results

Shown in table 6.2 are results from two different runs. As seen, oil rate of the eight base jet pump wells fell by 155 bopd, while the esp conversion itself resulted in an addition of 324 bopd. Adding an impact on the eight base wells and benefit for jet pump conversion results in a net positive of 169 bopd.

Chapter 7: Conclusion

A new method of optimizing power fluid in jet pump oil wells is established and explained. The algorithm uses a reduced Newton direction with active set constraints for continuous optimization. Constraints are set up to handle a total power fluid limit as well as non-negative limit for each well. If desired, constraints could easily be added for minimum and maximum allowable power fluid per well.

The optimization algorithms are built on top of numerical methods for modeling fluid flow through jet pumps. Numerical methods capture the reservoir fluids density changes related to pressure and flow limits encountered from sonic velocity constraints. This is a significant improvement from current industry methodologies that use analytical methods by Petrie, Wilson, and Smart [15]. Since the calculations required to apply numerical methods are large, a computer program was developed to handle optimization and jet pump modeling.

A field example of an eight jet pump well network was presented. The optimization scheme helped the field operator answer the question of whether an esp well should be converted to jet pump. The operator was unsure of how the well would perform on jet pump and its impact to the other existing producers. Analysis showed that converting the well resulted in a net improvement on oil production, and the project was sanctioned.

Optimization and modeling proposed in this paper marks an important transition in jet pump applications. As more oil fields target cold, shallow, viscous reservoirs, it is expected that the use of jet pumps and their associated networks will increase. Authors of this paper hope it helps operators allocate power fluid volumes for jet pump oil wells. It is also our hope that this paper inspires others to improve the methodology discussed above.

Appendix A: Throat Entrance Equation

The following appendix provides a derivation for the jet pump throat entry, equation (3.3) and (4.1), from the main document. The jet pump energy, equation (3.2), is integrated across from suction to the throat entry.

$$\int_{su}^{te} \frac{dP}{\rho} + \int_{su}^{te} V dV + \int_{su}^{te} dF = 0 \tag{A.1}$$

The following simplifying assumptions are applied.

1. Velocity of the fluid at suction conditions is negligible
2. Friction is represented by Cunningham friction coefficients

The following complexities are maintained.

1. Density and differential pressure relationship of the multiphase mixture

$$\int_{su}^{te} \frac{dP}{\rho} + \frac{V_{te}^2}{2} - \frac{\cancel{V_{su}^2}}{\cancel{2}} + K_{te}\frac{V_{te}^2}{2} = 0 \tag{A.2}$$

Rewriting in the simplest analytical form.

$$\int_{su}^{te} \frac{dP}{\rho} + \frac{V_{te}^2}{2} * (1 + K_{te}) = 0 \tag{A.3}$$

The trapezoid rule is applied as a numerical integration approximation to describe the density of the oil mixture with changes in pressure. ΔP is a user input that controls the granularity of the numerical approximation.

$$\frac{\Delta P}{2} \sum_{k=su}^{te} (\frac{1}{\rho_k} + \frac{1}{\rho_{k+1}}) + \frac{V_{te}^2}{2} * (1 + K_{te}) = 0 \tag{A.4}$$

Appendix B: Nozzle Equation

The following appendix provides a derivation for jet pump nozzle, equation (3.4) from the main document. The jet pump energy, equation (3.2), is integrated across from the nozzle inlet to the nozzle tip.

$$\int_{ni}^{nz} \frac{dP}{\rho} + \int_{ni}^{nz} V dV + \int_{ni}^{nz} dF = 0 \tag{B.1}$$

The following simplifying assumptions are applied.

1. Density of the power fluid is incompressible water
2. Velocity of the nozzle inlet is negligible
3. Friction is represented by Cunningham friction coefficients

$$\frac{P_{nz}}{\rho_{nz}} - \frac{P_{ni}}{\rho_{nz}} + \frac{V_{nz}^2}{2} - \frac{\cancel{V_{ni}^2}}{\cancel{2}} + K_{nz}\frac{V_{nz}^2}{2} = 0 \tag{B.2}$$

Multiplying through by the density and writing the equation in terms of $\mathrm{P_{nz}}$.

$$P_{nz} = P_{ni} - \frac{\rho_{nz} V_{nz}^2}{2} * (1 + K_{nz}) \tag{B.3}$$

The pressure at the nozzle is assumed to be the same as the pressure at the throat entrance, giving the final version of the nozzle equation.

$$P_{te} = P_{ni} - \frac{\rho_{nz} V_{nz}^2}{2} * (1 + K_{nz}) \tag{B.4}$$

Appendix C: Throat Equation

The following appendix provides a derivation for the jet pump throat mixing, equation (3.5) from the main document. The fixed control volume linear momentum equation is used to represent the nozzle. Section 3.4 *Linear Momentum Equation* from White [27] should be consulted for more information.

$$\sum \mathbf{F} = \frac{d}{dt} \int_{CV} V \rho \, d\forall \; + \int_{CS} V \rho \, (V \cdot \hat{n}) \, dA \tag{C.1}$$

For a steady state and one dimensional flow, the equation simplifies to.

$$\sum \mathbf{F} = \sum (\dot{m} V)_{out} - \sum (\dot{m} V)_{in} \tag{C.2}$$

Writing in terms of the jet pump throat. Where τA_w is the shear force imparted on the throat wall by the fluid.

$$P_{te} A_{th} - P_{tm} A_{th} - \tau A_w = \dot{m}_{tm} V_{tm} - \dot{m}_{nz} V_{nz} - \dot{m}_{te} V_{te} \tag{C.3}$$

According to Cunningham [1] the shear stress along the wall is rewritten as:

$$\frac{\tau A_w}{A_{th}} = \frac{\rho_{tm} V_{tm}^2 K_{th}}{2} \tag{C.4}$$

Placing the shear stress on the right and substituting in (C.4) yields the throat force balance.

$$P_{te} - P_{tm} = \frac{\rho_{tm} V_{tm}^2 K_{th}}{2} + \frac{\dot{m}_{tm} V_{tm}}{A_{th}} - \frac{\dot{m}_{nz} V_{nz}}{A_{th}} - \frac{\dot{m}_{te} V_{te}}{A_{th}} \tag{C.5}$$

Appendix D: Diffuser Equation

The following appendix provides a derivation for the jet pump diffuser, equation (3.6), from the main document. The jet pump energy, equation (3.2), is integrated across from the throat mixture to the diffuser.

$$\int_{tm}^{di} \frac{dP}{\rho} + \int_{tm}^{di} V dV + \int_{tm}^{di} dF = 0 \tag{D.1}$$

The following simplifying assumptions are applied.

1. Friction is represented by Cunningham friction coefficients

The following complexities are maintained.

1. Velocity of the throat mixture
2. Density and differential pressure relationship of the multiphase mixture

$$\int_{tm}^{di} \frac{dP}{\rho} + \frac{V_{di}^2}{2} - \frac{V_{tm}^2}{2} - K_{di}\frac{V_{tm}^2}{2} = 0 \tag{D.2}$$

Rewriting in the simplest analytical form.

$$\int_{tm}^{di} \frac{dP}{\rho} + \frac{V_{di}^2}{2} - \frac{V_{tm}^2}{2} * (1 + K_{di}) = 0 \tag{D.3}$$

The trapezoid rule is applied as a numerical integration approximation to describe the density of the oil mixture with changes in pressure. ΔP is a user input that controls the granularity of the numerical approximation.

$$\frac{\Delta P}{2} \sum_{k=tm}^{di} (\frac{1}{\rho_k} + \frac{1}{\rho_{k+1}}) + \frac{V_{di}^2}{2} - \frac{V_{tm}^2}{2} * (1 + K_{di}) = 0 \tag{D.4}$$

Appendix E: Gradient of the Throat Entry Energy vs Pressure

The following appendix provides a derivation for equation (4.2) from the main document. Three fundamental equations are used when assessing change in energy of the throat entrance versus the change in pressure. The equations are the differential friction-less throat entry energy (E.1), differential conservation of mass (E.2), and sonic velocity of a fluid (E.3).

$$dE_{te} = \frac{dP}{\rho} + VdV \tag{E.1}$$

$$\frac{d\rho}{\rho} + \frac{dV}{V} + \frac{dA}{A} = 0 \tag{E.2}$$

$$a^2 = \frac{dP}{d\rho} \tag{E.3}$$

The fluid sonic velocity (E.3) is written as $dP = a^2 d\rho$ and substituted into $\mathrm{dE_{te}}$ (E.1) for dP.

$$dE_{te} = \frac{a^2 d\rho}{\rho} + VdV \tag{E.4}$$

The entire equation is divided through by a^2 and the last term is multiplied by V/V.

$$\frac{dE_{te}}{a^2} = \frac{d\rho}{\rho} + \frac{V^2}{a^2}\frac{dV}{V} \tag{E.5}$$

In this specific application the analysis is exactly at the throat entry and investigating how its energy changes with pressure. As such, the differential area term is 0 in equation (E.2). The equation is rewritten by moving $d\rho/\rho$ to the right side.

$$\frac{dV}{V} = -\frac{d\rho}{\rho} \tag{E.6}$$

In equation (E.5) it is recognized that $\mathrm{Ma}^2 = V^2/a^2$. Additionally equation (E.6) is substituted into (E.5).

$$\frac{dE_{te}}{a^2} = \frac{d\rho}{\rho} - \mathrm{Ma}^2\frac{d\rho}{\rho} \tag{E.7}$$

The parameter $d\rho/\rho$ is factored out of equation (E.7) and then divided by $d\rho$.

$$\frac{dE_{te}}{a^2 d\rho} = \frac{1}{\rho}(1 - \mathrm{Ma}^2) \tag{E.8}$$

Equation (E.3), the sonic velocity, is substituted into equation (E.8) in the form $a^2 d\rho = dP$.

$$\frac{dE_{te}}{dP} = \frac{1}{\rho}(1 - \mathrm{Ma}^2) \tag{E.9}$$

Equation (E.9) provides the final form and describes the behavior of $\mathrm{dE_{te}}$ versus changes in pressure. It should noted that the original form of $\mathrm{dE_{te}}$ was idealized, as friction was not included. Nonetheless, equation (E.9) demonstrates that the slope of E_{te} vs pressure will change once the sonic boundary is activated. This matches performance found in the numerical analysis of E_{te} and traditional analysis of flow properties at sonic conditions [27].

Appendix F: PVT, Sonic and Multiphase Flow Correlations

The following appendix provides details of the correlations and equations used for PVT properties, sonic velocity and flow regime in piping systems.

F.1 Oil Properties

A black oil model with empirical data from a flash vaporization process is used. An empirical model based on flash vaporization process was chosen because "gas liberated from oil in a PVT cell during pressure decline remains in contact with the oil from which it was liberated, similar to what is normally encountered in pipe flow" Al-Safran and Brill [28, Page 283].

A black oil model is defined by the inputs below.

1. In-situ Pressure - p
2. Bubble Point Pressure - p_b
3. In-situ Temperature - T
4. Oil API Gravity - γ_{api}
5. Gas Gravity - γ_g

It should be noted that the equations below are valid for the specific black oil model referenced, but a user may want to use a different model. This is why the flexibility of a numerical method is advantageous to handle the output for a wide range of black oil models.

1. Gas Solubility in Oil: R_s
   (a) Above Bubblepoint: Saturated oil, where $p \geq p_b$ which is the oil bubble point.

$$R_s = R_p$$

   (b) Below Bubblepoint: Kartoatmodjo and Schmidt [29]

$$R_s = 0.05958\gamma_g^{0.7972} p^{1.0014} 10^{\frac{13.1405\gamma_{api}}{T+460}}$$

for $\gamma_{api} \leq 30$. A second correlation is provided in the reference for $\gamma_{api} > 30$.

2. Oil Compressibility: c_o

   (a) Above Bubblepoint: Vasquez and Beggs [30]

$$c_o = \frac{5R_s + 17.2T - 1180\gamma_g + 12.61\gamma_{api} - 1433}{(p + 14.7) * 10^5}$$

   (b) Below Bubblepoint: McCain, Rollins, and Lanzi [31]

$$\ln c_o = -7.633 - 1.497 \ln(p + 14.7) + 1.115 \ln T + 0.533 \ln \gamma_{api} + 0.184 \ln R_s$$

3. Formation Volume Factor: B_o

   (a) Above Bubblepoint: Vasquez and Beggs [30]

$$B_o = B_{ob} \exp[c_o(p_b - p)]$$

   where B_{ob} is the formation volume volume at $p = p_b$

   (b) Below Bubblepoint: Kartoatmodjo and Schmidt [29]

$$F = R_s^{0.755} * \gamma_g^{0.25} * \gamma_o^{-1.5} + 0.45T$$

$$B_o = 0.98496 + 0.0001F^{1.5}$$

4. Oil Density: ρ_o

   (a) Above Bubblepoint:

$$\rho_o = \rho_{ob} \exp[c_o(p_b - p)]$$

   where ρ_{ob} is the density at $p = p_b$

   (b) Below Bubblepoint:

$$\rho_o = \frac{62.4\gamma_o + 0.0136R_s\gamma_g}{B_o}$$

5. Oil Viscosity: μ_o

(a) Dead Oil: Kartoatmodjo and Schmidt [29]

$$\mu_{od} = (16 \times 10^8) \cdot T^{-2.8177} \log(\gamma_{api})^{(5.7526 \log(T) - 26.9718)}$$

(b) Above Bubblepoint: Kartoatmodjo and Schmidt [29]

$$\mu_o = 1.00081\mu_{ob} + 0.001127(p - p_b)(-0.006517\mu_{ob}^{1.8148} + 0.038\mu_{ob}^{1.59})$$

where μ_{ob} is the viscosity at the $p = p_b$.

(c) Below Bubblepoint: Kartoatmodjo and Schmidt [29]

$$\mu_o = -0.06821 + 0.9824f + 0.0004034f^2$$

$$f = [0.2001 + 0.8428(10^{-0.000845R_s})]\mu_{od}^{(0.43+0.5165y)}$$

$$y = 10^{-0.00081R_s}$$

6. Surface Tension: σ_o

(a) Dead Oil: Abdul-Majeed and Abu Al-Soof [32]

$$\sigma_{od} = A(38.085 - 0.259\gamma_{api})$$

$$A = 1.11591 - 0.00305 * \frac{5}{9}(T - 32)$$

(b) Live Oil: Abdul-Majeed and Abu Al-Soof [32]

$$\sigma_o = \frac{\sigma_{od}}{1 + 0.02549R_s^{1.0157}}$$

if $R_s < 50\ \frac{m^3}{m^3}$

$$\sigma_o = \sigma_{od} * 32.0436R_s^{-1.1367}$$

if $R_s \geq 50\ \frac{m^3}{m^3}$

F.2 Gas Properties

For the free gas in the mixture, the following correlations are used. They are simplifications that have performed well for natural gases with low carbon dioxide and hydrogen sulfide.

1. Gas Pseudo Critical Properties: Sutton [33]

$$p_{pc} = 756.8 - 131.07\gamma_g - 3.6\gamma_g^2$$

$$T_{pc} = 169.2 - 349.5\gamma_g - 74.0\gamma_g^2$$

2. Gas Z-Factor, Z

$$Z = 1 - m * p_{pr} + n * p_{pr}^2 + 0.0003p_{pr}^3$$

$$m = 0.51T_{pr}^{-4.133}$$

$$n = 0.038 - 0.036T_{pr}^{0.5}$$

   where p_{pr} and T_{pr} are the pseudo critical reduced properties.

3. Gas Density, ρ_g

$$\rho_g = \frac{(p + 14.7) * MW}{Z * R * (T + 460)}$$

4. Gas Compressibility, c_g

$$c_g = \frac{1}{p} - \frac{1}{Z}\left(\frac{dZ}{dp}\right)_T$$

5. Gas Viscosity, μ_g: Lee, Gonzalez, and Eakin [34]

$$\mu_g = 10^{-4}K \exp\left[X\left(\frac{\rho_g}{62.4}\right)^Y\right]$$

$$K = \frac{(9.4 + 0.02MW)(T + 460)^{1.5}}{209 + 19MW + T + 460}$$

$$X = 3.5 + \frac{986}{T + 460} + 0.01MW$$

$$Y = 2.4 - 0.2X$$

F.3 Water Properties

For water, constants are assumed through out the process which are shown below. Entrained gas inside water is assumed to be negligible.

1. Water Density, $\rho_w = 63.6\ lb_m/ft^3$
2. Water Compressibility, $c_w = 4.5 \times 10^{-4}$ MPa^{-1}
3. Water Viscosity, $\mu_w = 0.75\ cP$
4. Water Surface Tension, $\sigma_w = 72.8$ dyne/cm

F.4 Mass Fractions

A mixture is defined using a formation gas oil ratio (fgor) and watercut (wc). The fgor and wc are used in conjunction with fluid densities to calculate the mass fractions of the oil, water and gas. Standard conditions is defined as $60°F$ and 0 psig and highlighted by std.

1. Mass based gas solubility, M_{Rs}

$$M_{Rs} = R_s \frac{7.48\ \rho_{g,std}}{42\ \rho_{o,std}}$$

2. Mass based fgor, M_{fgor}

$$M_{fgor} = fgor \frac{7.48\ \rho_{g,std}}{42\ \rho_{o,std}}$$

3. Mass based watercut, M_{wc}

$$M_{wc} = \frac{wc\ \rho_{w,std}}{wc\ \rho_{w,std} + (1 - wc)\ \rho_{o,std}}$$

4. Mass based formation gas to liquid ratio, M_{fglr}

$$M_{fglr} = fgor \frac{7.48\ \rho_{g,std}\ (1 - wc)}{42\ wc\ \rho_{w,std} + (1 - wc)\ \rho_{o,std}}$$

5. Mass fraction of gas, x_g

$$x_g = \frac{M_{fglr}}{1 + M_{fglr}}$$

6. Mass fraction of oil, x_o

$$x_o = \frac{1 - M_{wc}}{1 + M_{fgor}\,(1 - M_{wc})}$$

7. Mass fraction of water, x_w

$$x_w = 1 - x_o - x_g$$

8. Mass fraction of gas in oil, x_{rs}

$$x_{rs} = x_o\, M_{Rs}$$

9. Update gas and oil mass fractions

$$x_g = x_g - x_{rs}$$

$$x_o = 1 - x_w - x_g$$

Mass and volume fractions from 100 to 2500 psig were calculated are compared against industrial process modeling software hysys. It was found that mass and volume fractions calculated were within 6% of what hysys calculated.

F.5 Mixture Properties

Mixture properties are assumed homogeneous for density, viscosity, surface tension, compressibility. Where x is a mass fraction in the mixture of either oil o, water w or gas g. A volume fraction is defined as y.

1. Mixture Density, ρ_{mix}

$$\frac{1}{\rho_{mix}} = \frac{x_o}{\rho_o} + \frac{x_w}{\rho_w} + \frac{x_g}{\rho_g}$$

2. Mixture Viscosity, μ_{mix}

$$\mu_{mix} = y_o\mu_o + y_w\mu_w + y_g\mu_g$$

3. Mixture Compressibility, c_{mix}

$$c_{mix} = y_o c_o + y_w c_w + y_g c_g$$

4. Liquid Surface Tension, σ_{liq}

$$\sigma_{liq} = \sigma_o \left(1 - f_w\right) + \sigma_w \, f_w$$

$$f_w = \frac{y_w}{y_o + y_w}$$

F.6 Sonic Velocity Properties

Properties required for predicting sonic velocity are fluid compressibility, c and fluid density, ρ. Mixture properties are used in the standard sonic velocity equation, displayed as equation (F.1).

$$a_{mix} = \sqrt{\frac{1}{c_{mix} \, \rho_{mix}}} \tag{F.1}$$

The Mach number is a dimensionless number that compares the velocity a fluid is flowing to its speed of sound, represented in equation (F.2).

$$Ma = \frac{v_{mix}}{a_{mix}} \tag{F.2}$$

Flow is described sonically by the categories listed below. The boundary limit for oil well jet pumps is a Mach value of 1 or below. Fluids can be accelerated to a value above Mach 1, but require a specialized device which has characteristics not found in a jet pump.

- Subsonic: $Ma \leq 0.8$
- Transonic: $0.8 < Ma < 1.2$
- Supersonic: $1.2 \leq Ma$

F.6.1 Sonic Velocity Example

A multiphase mixtures sonic velocity is less than the sonic velocities of it's individual components [22]. An example of this is a mixture of air and water. The individual components of air and water have a sonic velocity of 1100 and 5000 ft/s respectively. Combining these fluids in a 50/50 mixture results in a sonic velocity of 300 ft/s, nearly a quarter less than the sonic velocity of the air

by itself. This property of multiphase mixtures makes the likelihood of hitting the sonic velocity very plausible.

F.7 Flow Correlation

For multiphase flow the correlation chosen is Beggs and Brill [24]. The Beggs and Brill was chosen for its wide acceptance in industry and flexibility to be applied for horizontal, incline and vertical flow. For single phase Darcy-Weisbach equation for pressure drop in piping and the Serghide equation for friction coefficient.

Appendix G: Numerical Methods

The following is brief review of some of the numerical methods that appear in this document. The following is intended to be a refresher and cannot replace detailed references. For further information, please see [23].

G.1 Trapezoid Rule

The trapezoid rule is a numerical integration method that approximates the integral of a function $f(x)$ over an interval $[a, b]$ by dividing it into small trapezoids. The formula for the trapezoid rule with n equally spaced sub-intervals is:

$$\int_a^b f(x)\,dx \approx \frac{h}{2}\sum_{i=0}^{n}[f(x_i) + f(x_{i+1})] \quad \text{where} \quad h = \frac{b-a}{n}$$

An example function is shown below that is approximated with trapezoids.

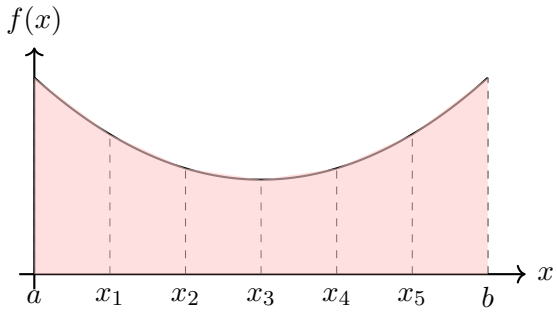

The function is a parabola of the form $f(x) = 1.25 + 0.3\dfrac{(x-3)^2}{2}$ The trapezoids are represented by the light red.

G.2 Newton Method - Root Finding

Newton's method is an iterative technique for solving equations $f(x) = 0$. Starting from an initial guess x_0, the update rule is:

$$x_{n+1} = x_n - \frac{f(x_n)}{f'(x_n)}$$

Where $f'(x)$ is the first derivative. Convergence is quadratic if the initial guess is close to the

root and $f'(x) \neq 0$.

G.3 Secant Method - Root Finding

The secant method is a modification of Newton's method that approximates the derivative using two points. The update rule is:

$$x_{n+1} = x_n - f(x_n)\frac{x_n - x_{n-1}}{f(x_n) - f(x_{n-1})}.$$

The method does not require $f'(x)$ but needs two initial guesses x_0 and x_1. Convergence is super linear at a rate of $r = 1.61$ if the initial guess is close to the root and $f(x_*) - f(x_{*-1}) \neq 0$.

G.4 Newton Method - Optimization

Newton's method can also be used to find critical points of a function $g(x)$. The critical points satisfy $g'(x) = 0$. The iterative update rule is:

$$x_{n+1} = x_n - \frac{g'(x_n)}{g''(x_n)}.$$

Here, $g'(x)$ is the first derivative, and $g''(x)$ is the second derivative of $g(x)$.

G.5 Newton Method - Multi Dimensions

Newton's method can be expanded to handle multiple dimensions iterations, where x is now a vector. For the optimization case where the target is $\nabla g(x) = 0$, this is written as:

$$x_{n+1} = x_n - \nabla^2 g(x_n)^{-1} \nabla g(x_n)$$

Where $\nabla^2 g(x_n)^{-1}$ is the inverse Hessian of the function and $\nabla g(x_n)$ is the gradient.

Appendix H: National Jet Pump Geometry

Nozzle No.	Nozzle Dia. inches	Throat No.	Throat Dia. inches
1	0.0553	1	0.0903
2	0.0628	2	0.1016
3	0.0705	3	0.1151
4	0.0798	4	0.1291
5	0.0903	5	0.1458
6	0.1016	6	0.1643
7	0.1145	7	0.1858
8	0.1291	8	0.2099
9	0.1458	9	0.2370
10	0.1643	10	0.2675
11	0.1858	11	0.3017
12	0.2099	12	0.3404
13	0.2370	13	0.3841
14	0.2675	14	0.4335
15	0.3017	15	0.4981
16	0.3404	16	0.5519
17	0.3841	17	0.6228
18	0.4335	18	0.7027
19	0.4981	19	0.7929
20	0.5519	20	0.8947

Table H.1: National Nozzle and Throat Sizes

Bibliography

[1] R. G. Cunningham, "Liquid jet pumps for two-phase flows," *Journal of Fluids Engineering*, vol. 117, no. 2, pp. 309–316, Jun. 1995. DOI: 10.1115/1.2817147.

[2] R. Merrill, V. Shankar, and T. Chapman, "Three-phase numerical solution for jet pumps applied to a large oilfield," in *Abu Dhabi International Petroleum Exhibition and Conference*, Nov. 2020. DOI: 10.2118/202928-MS.

[3] R. G. Cunningham, "The jet pump as a lubrication oil scavenge pump for aircraft engines," Wright Air Development Center, Technical Report, Jul. 1954.

[4] G. Flügel, "The design of jet pumps," National Advisory Committee for Aeronautics, Technical Report, Jul. 1941.

[5] C. J. Coberly, *Theory and Application of Hydraulic Oil Well Pumps*. Kobe Inc., 1961.

[6] N. L. Sanger, "Noncavitating performance of two low-area-ratio water jet pumps having throat lengths of 7.25 diameters," National Aeronautics and Space Administration, Technical Report, Mar. 1968.

[7] N. L. Sanger, "Cavitating performance of two low-area-ratio water jet pumps having throat lengths of 7.25 diameters," National Aeronautics and Space Administration, Technical Report, May 1968.

[8] R. G. Cunningham, A. G. Hansen, and T. Y. Na, "Jet pump cavitation," *Journal of Basic Engineering*, vol. 92, no. 3, pp. 483–492, Sep. 1970. DOI: 10.1115/1.3425040.

[9] P. Wilson, "Jet free pump: A progress report on two years of field performance," Kobe Inc., Technical Report, 1972.

[10] R. G. Cunningham and R. J. Dopkin, "Jet breakup and mixing throat lengths for the liquid jet gas pump," *Journal of Fluids Engineering*, vol. 96, no. 3, pp. 216–226, Sep. 1974. DOI: 10.1115/1.3447144.

[11] R. G. Cunningham, "Gas compression with the liquid jet pump," *Journal of Fluids Engineering*, vol. 96, no. 3, pp. 203–215, Sep. 1974. DOI: 10.1115/1.3447143.

[12] H. Petrie, "Jet pumping," in *The Technology of Artificial Lift Methods*, K. E. Brown, Ed. Petroleum Publishing Co., 1980, vol. 2b, ch. 6, pp. 453–481.

[13] J. E. Gosline and M. P. O'Brien, *The Water Jet Pump*. University of California Press, 1934.

[14] H. Petrie, P. Wilson, and E. Smart, "Jet pumping oil wells, part 1 design theory, hardware options and application considerations," *World Oil*, vol. 197, no. 6, Nov. 1983.

[15] H. Petrie, P. Wilson, and E. Smart, "Jet pumping oil wells, part 2 hand held computer programs for installation design," *World Oil*, vol. 198, no. 7, Dec. 1983.

[16] H. Petrie, P. Wilson, and E. Smart, "Jet pumping oil wells, part 3 how design calculations compare with actual field performance," *World Oil*, vol. 199, no. 8, Jan. 1984.

[17] B. Jiao, "Performance model for hydraulic jet pumping of two-phase fluids," Ph.D. dissertation, University of Tulsa, 1988.

[18] S. K. Verma, S. P. Ojha, M. Jha, *et al.*, "The importance of critical flow considerations in understanding jet pump performance: The mangala field," in *IPTC International Petroleum Technology Conference*, Dec. 2014. DOI: 10.2523/IPTC-18167-MS.

[19] N. Nishikiori, "Gas allocation optimization for continuous flow gas lift systems," M.S. thesis, University of Tulsa, 1989.

[20] F. Holland and B. R, "Fluid flow for chemical engineers," in 338 Euston Road, London NW1 3BH: Edward Arnold, 1995, ch. 6, pp. 189–190.

[21] J. Vogel, "Inflow Performance Relationships for Solution-Gas Drive Wells," *Journal of Petroleum Technology*, vol. 20, no. 01, pp. 83–92, Jan. 1968. DOI: 10.2118/1476-PA.

[22] D. Himr, V. Haban, and F. Pochyly, "Sound speed in the mixture water - air," in *Engineering Mechanics Conference*, Svratka, Czech Republic, May 2009.

[23] A. Gilat and V. Subramaniam, "Numerical methods for engineers and scientists 3rd ed.," in Wiley, 2013, ch. 9.

[24] G. Payne, C. Palmer, J. Brill, and H. Beggs, "Evaluation of inclined-pipe, two-phase liquid holdup and pressure-loss correlation using experimental data," *Journal of Petroleum Technology*, vol. 31, no. 09, Sep. 1979. DOI: 10.2118/6874-PA.

[25] L. Armijo, "Minimization of Functions having Lipschitz Continuous First Partial Derivatives," *Pacific Journal of Mathematics*, vol. 16, no. 01, Nov. 1966. DOI: 10.2140/pjm.1966.16.1.

[26] I. Griva, S. Nash, and A. Sofer, "Linear and Nonlinear Optimization 2nd Ed.," in SIAM Press, 2009, ch. 15.2 - 15.4, pp. 549–570.

[27] F. White, "Fluid mechanics 7th ed.," in 1221 Avenue of the Americas, New York, NY 10020: McGraw-Hill, 2011, ch. 9, pp. 622–623.

[28] E. M. Al-Safran and J. P. Brill, *Applied Multiphase Flow in Pipes and Flow Assurance*. Society of Petroleum Engineers, 2017. DOI: 10.2118/9781613994924.

[29] T. Kartoatmodjo and Z. Schmidt, "New correlations for crude oil physical properties," *Society of Petroleum Engineers*, 1991.

[30] M. Vasquez and H. Beggs, "Correlations for fluid physical property prediction," *Journal of Petroleum Technology*, vol. 32, no. 06, pp. 968–970, Jun. 1980. DOI: 10.2118/6719-PA.

[31] J. McCain William D., J. B. Rollins, and A. J. V. Lanzi, "The coefficient of isothermal compressibility of black oils at pressures below the bubblepoint," *SPE Formation Evaluation*, vol. 3, no. 03, pp. 659–662, Sep. 1988. DOI: 10.2118/15664-PA.

[32] G. H. Abdul-Majeed and N. B. Abu Al-Soof, "Estimation of gas–oil surface tension," *Journal of Petroleum Science and Engineering*, vol. 27, no. 3, pp. 197–200, 2000. DOI: 10.1016/S0920410500000589.

[33] R. P. Sutton, "Compressibility factors for high-molecular-weight reservoir gases," *SPE Annual Technical Conference and Exhibition*, Sep. 1985. DOI: 10.2118/14265-MS.

[34] A. L. Lee, M. H. Gonzalez, and B. E. Eakin, "The viscosity of natural gases," *Journal of Petroleum Technology*, vol. 18, no. 08, pp. 997–1000, Aug. 1966. DOI: 10.2118/1340-PA.